Computation of equilibrium states and bifurcations using interval analysis: Application to food chain models

C. Ryan Gwaltney, WenTao Luo, Mark A. Stadtherr [1]

Department of Chemical and Biomolecular Engineering, 182 Fitzpatrick Hall,
University of Notre Dame, Notre Dame IN 46556, USA

Abstract

Food chains and webs in the environment are highly nonlinear and interdependent systems. When these systems are modeled using simple sets of ordinary differential equations, these models can exhibit very rich and complex mathematical behaviors. We present here a new equation-solving technique for computing all equilibrium states and bifurcations of equilibria in food chain models. The method used is based on interval analysis, in particular an interval-Newton/generalized-bisection algorithm. Unlike the continuation methods often used in this context, the interval method provides a mathematical and computational *guarantee* that *all* roots of a nonlinear equation system are located. The technique is demonstrated using three different food chain models, and results of the computations are used to compare the models.

Keywords: Equilibrium states; Bifurcations; Food chain; Computational method; Interval analysis

---

1 Introduction

Food chain modeling provides challenges in the fields of both theoretical ecology and applied mathematics. Simple food chain models often display rich nonlinear mathematical behavior, including varying numbers and stability of equilibrium states and limit cycles, which change as the model parameters change. Many different model formulations are possible, depending on the

---

[1] Author to whom all correspondence should be addressed. Fax: (574) 631-8366; E-mail: markst@nd.edu

Paper accepted for Ecological Modelling *12 December 2006*

number of species being analyzed, the predation responses being used, whether age or fertility structure is of interest for a given species, and how resources are being modeled for the basal species. Analysis of food chain models is often performed by examining the parameter space of the model in one or more variables. This approach is referred to as bifurcation analysis, and it provides a powerful tool for concisely representing a large amount of information regarding both the number and stability of equilibrium states (steady states) and limit cycles in a model. In a two-parameter bifurcation diagram, the shape of bifurcation curves can elucidate the dependence, or lack there of, between model parameters, which in turn can provide information on their ecological relevance. Furthermore, both the shape and the order of bifurcation curves in a diagram can be used to make comparisons between different food chain models.

Determining the equilibrium states and bifurcations of equilibria in a nonlinear dynamical system is often a challenging problem, and great effort can be expended in analyzing even a relatively simple food chain model with nonlinear functional responses. For some simple systems, or specific parts of more complex ones, analytic techniques and isocline analysis may be useful. However, for more complex problems, numerical continuation methods are the predominant computational tools, with packages such as AUTO (Doedel et al., 2002), MATCONT (Dhooge et al., 2003) and others being particularly popular in this context. Continuation methods can be quite reliable, especially in the hands of an experienced user. However, continuation methods are initialization dependent and thus provide no guarantee that all equilibrium states and all bifurcations of equilibria will be found. Effective use of continuation methods may require some *a priori* understanding of system behavior in order to provide the initializations needed to determine a complete bifurcation diagram. In this paper, we describe an alternative approach for computing equilibrium states and bifurcations of equilibria, and apply this approach to an analysis and comparison of food chain models. This approach is based on interval mathematics, in particular an interval-Newton approach combined with generalized bisection, and provides a *mathematical and computational guarantee* that *all* equilibrium states and bifurcations of equilibria will be located, without need for initializations or *a priori* insights into system behavior. There are other dynamical features of interest in food chain models, such as limit cycles (and their bifurcations); however, our attention here will be limited to equilibrium states and their bifurcations. Interval methodologies have been successfully applied to the problem of locating equilibrium states and singularities in traditional chemical engineering problems, such as reaction and reactive distillation systems. Examples of these applications are given in Schnepper and Stadtherr (1996), Gehrke and Marquardt (1997), Bischof et al. (2000), and Mönnigmann and Marquardt (2002).

Many simple two species food chain models have been thoroughly explored, while recent attention has been focused on models with three or more trophic levels. Two tritrophic food chain models have received considerable attention in the field of theoretical ecology (Kooi, 2003). These models both feature Holling Type II predation responses, but one is embedded in a chemostat while the other features a prey that grows logistically in the absence of a predator. These models are often referred to as Canale's chemostat model and the (tritrophic) Rosenzweig-MacArthur model, respectively. In this paper, we will consider as examples these two models, along with a third, experimentally-verified model (Fussmann et al., 2000) that has recently been introduced into the literature. This third model involves a planktonic rotifer feeding on a unicellular green algae. Nitrogen is the limiting resource for the algae, and is modeled using a chemostat. The planktonic rotifer is modeled as a fertility-structured population, and consumes algae according to the Holling Type II functional response. These three food chain models share some fundamental similarities (all use the Holling Type II response, two are embedded in a chemostat), but they feature major differences, too. We will demonstrate the interval method by using it to compute bifurcation diagrams for these three example systems. Bifurcation analysis is then used to determine what qualitative effects the similarities and differences between these models have on the number and stability of equilibrium states.

Though it is not the primary focus here, our overall interest in ecological modeling is motivated by its use as one tool in studying the impact on the environment of the industrial use of newly discovered materials. Clearly it is preferable to take a proactive, rather than reactive, approach when considering the safety and environmental consequences of using new compounds. Of particular interest is the potential use of room temperature ionic liquid (IL) solvents in place of traditional solvents (Brennecke and Maginn, 2001). IL solvents have no measurable vapor pressure (i.e., they do not evaporate) and thus, from a safety and environmental viewpoint, have several potential advantages relative to the traditional volatile organic compounds (VOCs) used as solvents, including elimination of hazards due to inhalation, explosion and air pollution. However, ILs are, to varying degrees, soluble in water; thus if they are used industrially on a large scale, their entry into the environment via aqueous waste streams is of concern. The effects of trace levels of ILs in the environment are today not well known and thus must be further studied. Ecological modeling provides a means for studying the impact of such perturbations on a localized environment by focusing not just on single-species toxicity information, but rather on the larger impacts on the food chain and ecosystem (Bartell et al., 1992). Of course, ecological modeling is just one part of a much larger suite of tools, including toxicological (e.g.: Bernot et al., 2005a,b; Ranke et al., 2004; Stepnowski et al., 2004), microbiological (e.g.: Docherty and Kulpa, 2005; Pernak et al., 2003) and other (e.g.: Ropel et al., 2005; Gorman-Lewis and Fine, 2004) studies, that must be used in addressing this issue.

In the next section, we will briefly introduce the food chain models used as examples and we will formulate the nonlinear equation systems that must be solved in order to locate the equilibrium states and bifurcations of equilibria. In Section 3, a brief introduction to interval mathematics is given and the computational method is summarized. In Section 4, we apply the computational technique to compute bifurcation diagrams for the three example models of interest, and use these results to compare the models. In Section 5, we conclude and provide remarks on the advantages, applicability and limitations of the computational method presented.

2 Problem Formulation

2.1 Rosenzweig-MacArthur Model

The tritrophic Rosenzweig-MacArthur food chain model has been frequently studied in the field of theoretical ecology (Hastings and Powell, 1991; Abrams and Roth, 1994; Klebanoff and Hastings, 1994; Kuznetsov and Rinaldi, 1996; De Feo and Rinaldi, 1997; Gragnani et al., 1998; Kooi, 2003; Moghadas and Gumel, 2003). This food chain consists of a prey, predator, and superpredator. The prey is modeled using a logistic growth function, while the predators and superpredators consume biomass according to the Holling Type II, or hyperbolic, response function. This functional response is mathematically more complex than a simple linear response, but it provides a leveling-off (saturation) effect as prey abundance increases. Thus, it is a more realistic model of behavior observed in the environment. The model is given by the following balance equations:

$$\frac{dx_1}{dt} = x_1 \left[r \left(1 - \frac{x_1}{K} \right) - \frac{a_2 x_2}{b_2 + x_1} \right] \tag{1}$$

$$\frac{dx_2}{dt} = x_2 \left[e_2 \frac{a_2 x_1}{b_2 + x_1} - \frac{a_3 x_3}{b_3 + x_2} - d_2 \right] \tag{2}$$

$$\frac{dx_3}{dt} = x_3 \left[e_3 \frac{a_3 x_2}{b_3 + x_2} - d_3 \right]. \tag{3}$$

Here x_1, x_2, and x_3 are the biomasses of the prey, predator, and superpredator populations, respectively. The (nonnegative) parameters a_i, b_i, d_i, and e_i are the maximum predation rate, half-saturation constant, density-dependent death rate, and predation efficiency of the prey ($i = 1$), predator ($i = 2$), and superpredator ($i = 3$) species. The parameter r is the prey growth rate constant and K is the prey carrying capacity. The carrying capacity represents the maximum amount of prey biomass that the system can support in absence of a predator. As the prey population increases, the rate of growth declines until reaching the carrying capacity, at which point the rate of growth becomes zero. Positive terms on the right-hand sides of Eqs. (1–3) represent organism growth, while negative terms represent loss of organisms due to predation and death.

2.2 Canale's Chemostat Model

Canale's chemostat model is a tritrophic (prey, predator, superpredator) food chain model that is very similar to the Rosenzweig-MacArthur model presented in Section 2.1. The difference is that Canale's model is embedded in a chemostat, which is a constant volume system with constant flow in and out. The predator and superpredator grow by consuming the prey and predator species, respectively, while the prey grows by consuming nutrients in the chemostat. The rate at which the prey, predator, and superpredator consume food is modeled by the Holling Type II, or hyperbolic, functional response. There is a constant flow through the chemostat, which carries nutrients into the system, and which carries nutrients and organisms out of the system. Chemostat models are generally believed to be superior to logistic models in terms of resource/consumer interactions. Studies have compared logistic prey growth with chemostat-based food chains using both model formalisms and bifurcation diagrams. Several examples in literature utilize bifurcation diagrams to compare the behavior predicted by these different food chain models (Kooi et al., 1997b, 1998; Gragnani et al., 1998).

Canale's chemostat model is given by the following balance equations:

$$\frac{dx_0}{dt} = D(x_n - x_0) - \frac{a_1 x_0 x_1}{b_1 + x_0} \tag{4}$$

$$\frac{dx_1}{dt} = x_1 \left[e_1 \frac{a_1 x_0}{b_1 + x_0} - \frac{a_2 x_2}{b_2 + x_1} - d_1 - \varepsilon_1 D \right] \tag{5}$$

$$\frac{dx_2}{dt} = x_2 \left[e_2 \frac{a_2 x_1}{b_2 + x_1} - \frac{a_3 x_3}{b_3 + x_2} - d_2 - \varepsilon_2 D \right] \tag{6}$$

$$\frac{dx_3}{dt} = x_3 \left[e_3 \frac{a_3 x_2}{b_3 + x_2} - d_3 - \varepsilon_3 D \right] . \tag{7}$$

Here x_0 is the nutrient concentration in the system and x_1, x_2, and x_3 are the biomasses of the prey, predator, and superpredator populations, respectively. The (nonnegative) parameters a_i, b_i, d_i, and e_i are the maximum predation rate, half-saturation constant, density-dependent death rate, and predation efficiency of the prey ($i = 1$), predator ($i = 2$), and superpredator ($i = 3$) species. The parameter x_n is the nutrient concentration flowing into the system, and the parameter D is the inflow rate (equal to the outflow rate). The term $\varepsilon_i D$ is the density-dependent washout rate of species i. The constant $\varepsilon_i \in [0, 1]$ quantifies how well a species is able to resist washout. For instance, if $\varepsilon_i = 1$, the organism will be unable to resist washout. An example of such a species would be a unicellular algae. Conversely, if $\varepsilon_i = 0$, that organism is completely resistant to washout. Positive terms on the right-hand sides of Eqs. (4–7) represent inflow of nutrient and organism growth. Negative terms represent outflow and consumption of nutrient, and loss of organisms due to predation, wash out and death. This model has received considerable attention in the field of theoretical ecology (Kooi et al., 1997a; Boer et al., 1998; Gragnani et al., 1998; Kooi, 2003; El-Sheikh and Mahrouf, 2005).

2.3 Experimentally-Verified Algae-Rotifer Model

Fussmann et al. (2000) have presented a food chain model consisting of an age-structured population of planktonic rotifers, *Brachionus calyciflorus*, feeding on unicellular green algae, *Chlorella vulgaris.* Nitrogen is the resource that limits algal growth in this chemostat system. By varying both the inflow nutrient concentration as well as the dilution rate in the experimental system, Fussmann et al. (2000) were able to observe both steady-state and oscillatory behavior in the species populations. By using data from both literature and from experiments, Fussmann et al. (2000) constructed a simple nonlinear model that was able to qualitatively predict both the steady-state and oscillatory behavior observed in the experimental setup. Furthermore, this model was able to predict the points at which the populations transition from a stable state to an oscillatory state. This model is given by the following balance equations:

$$\frac{dN}{dt} = \delta(N_i - N) - \frac{b_C NC}{K_C + N} \tag{8}$$

$$\frac{dC}{dt} = \frac{b_C NC}{K_C + N} - \frac{1}{\varepsilon}\frac{b_B CB}{K_B + C} \tag{9}$$

$$\frac{dR}{dt} = \frac{b_B CR}{K_B + C} - (\delta + m + \lambda)\, R \tag{10}$$

$$\frac{dB}{dt} = \frac{b_B CR}{K_B + C} - (\delta + m)\, B. \tag{11}$$

Here N is the concentration of nitrogen in the system, C is the concentration of the algae (*Chlorella vulgaris*), R is the concentration of the reproducing rotifers, and B is the total rotifer (*Brachionus calyciflorus*) concentration. N_i is the concentration of nitrogen in the inflow medium while δ is the constant inflow rate in the system (equal to the outflow rate). b_C and b_B are the maximum birth rates of *Chlorella* and *Brachionus*, respectively, while K_C and K_B are the half-saturation constants of *Chlorella* and *Brachionus*, respectively. ε is the assimilation efficiency of *Brachionus*, and m is the mortality rate of *Brachionus*. As mentioned previously, the rotifer population is age-structured. The reproducing rotifers, R, comprise a subset of the total rotifer population, B. Growth in the rotifer population occurs only in the reproducing rotifer population. However, the entire rotifer population continues to consume algal biomass. Non-reproducing rotifers must continue to consume algae in order to replace biomass lost to respiration and excretion. After a period of time the reproducing rotifers stop producing offspring, and this is represented by λ, which is the fecundity decay rate. Since this model was experimentally verified, at least qualitatively, it provides an interesting basis of comparison to both Canale's model and the Rosenzweig-MacArthur model.

2.4 Equilibrium States

The equilibrium states (steady states) in a food chain are defined by the condition

$$\frac{d\boldsymbol{x}}{dt} = \boldsymbol{f}(\boldsymbol{x}) = \boldsymbol{0}, \tag{12}$$

which in this case is also subject to the feasibility condition

$$\boldsymbol{x} \geq \boldsymbol{0}. \tag{13}$$

Once all of the model parameters have been specified, Eq. 12 represents an $n \times n$ system of nonlinear equations which can be solved for the equilibrium states. In general, equation systems of this type, as they arise in the modeling of food chains, may have multiple solutions, and the number of equilibrium states may be unknown *a priori*. For simple models, it may be possible to solve for many of the equilibrium states analytically, and some states will not satisfy Eq. 13 and thus will be infeasible. For more complex models, however, a computational method is needed that is capable of finding, with certainty, all the feasible solutions of the nonlinear equation system, or any algebraic reduction thereof.

Determining the stability of an equilibrium state is accomplished by linearizing the model about the steady state and examining the eigenvalues that characterize the form of the solution to the linearized model. These are the eigenvalues of the Jacobian matrix of the model equations $\boldsymbol{f}(\boldsymbol{x})$ with respect to the state variables $\boldsymbol{x}$, or $J = \delta \boldsymbol{f}/\delta \boldsymbol{x}$, evaluated at the steady-state values of the state variables. In order for the equilibrium state to be stable, each of these eigenvalues must have a negative real part. If any of the real parts are nonnegative, then the equilibrium state cannot be classified as an attractor.

2.5 Bifurcations

A bifurcation is a change in the topological type of the phase portrait as one or more model parameters are varied. Bifurcations of interest here occur at parameter values where the number or stability of equilibrium states change (Kuznetsov, 1998). We are primarily interested in three types of codimension-one bifurcations, namely fold, transcritical and Hopf, and two types of codimension-two bifurcations, namely double-fold (or double-zero) and fold-Hopf. The "codimension" of a bifurcation indicates the number of additional conditions required to specify the particular type of bifurcation, and thus the number of parameters that must be allowed to vary. Thus, to find a codimension-one bifurcation, one additional condition must be given, and one parameter (which we denote as α) is allowed to vary, and to find a codimension-two bifurcation, two additional conditions must be given, and two parameters (α, β) are allowed to vary. Several detailed treatments of bifurcation analysis are available (e.g.: Seydel, 1988; Kuznetsov, 1998; Govaerts, 2000).

When a fold or transcritical bifurcation of equilibria occurs, two equilibria "collide" as the bifurcation parameter is varied. This collision results in either an exchange of stability (transcritical) or mutual annihilation of two equilibria (fold). Mathematically, when an equilibrium state undergoes either a fold or transcritical bifurcation, an eigenvalue of its Jacobian is zero (Govaerts, 2000). Since the determinant of a matrix is equal to the product of its eigenvalues, the determinant of the Jacobian will be zero at a fold or transcritical bifurcation, thereby providing a convenient test function (Kuznetsov, 1998). Thus, to locate fold or transcritical bifurcations of equilibria, the equilibrium condition can be augmented with the additional condition $\det[J(\boldsymbol{x}, \alpha)] = 0$ and additional variable α, the bifurcation parameter. This gives the augmented equation system

$$\frac{d\boldsymbol{x}}{dt} = \boldsymbol{f}(\boldsymbol{x}, \alpha) = 0 \tag{14}$$

$$\det[J(\boldsymbol{x}, \alpha)] = 0. \tag{15}$$

The augmented system is then solved to find any fold and transcritical bifurcations of equilibria, along with the corresponding value or values of α.

When a single equilibrium state changes stability as a model parameter is varied, this corresponds to a Hopf bifurcation. Mathematically, when an equilibrium state undergoes a Hopf bifurcation, its Jacobian has a pair of complex conjugate eigenvalues whose real parts are zero. Thus, there must be a pair of eigenvalues that sums to zero. According to Stephanos's theorem (Kuznetsov, 1998), for an $N \times N$ matrix J with eigenvalues $\lambda_1, \lambda_2, \ldots, \lambda_N$, the bialternate product $J \odot J$ has eigenvalues $\lambda_i \lambda_j$ and the bialternate product $2J \odot I$ has eigenvalues $\lambda_i + \lambda_j$. Thus, to locate a Hopf bifurcation, the equilibrium condition can be augmented (Kuznetsov, 1998; Govaerts, 2000) with the additional condition $\det[2J(\boldsymbol{x}, \alpha) \odot I] = 0$. This gives the augmented equation system

$$\frac{d\boldsymbol{x}}{dt} = \boldsymbol{f}(\boldsymbol{x}, \alpha) = 0 \tag{16}$$

$$\det[2J(\boldsymbol{x}, \alpha) \odot I] = 0. \tag{17}$$

The augmented system is then solved to find any Hopf bifurcations, along with the corresponding value or values of α. The bialternate product of two $N \times N$ matrices A and B is an $M \times M$ matrix denoted by $A \odot B$ whose rows are labeled by the multiindex (p, q) where $p = 2, 3, \ldots, N$ and $q = 1, 2, \ldots, p-1$, whose columns are labeled by the multiindex (r, s) where $r = 2, 3, \ldots, N$ and $s = 1, 2, \ldots, r-1$, where $M = N(N-1)/2$, and whose elements are given by

$$(A \odot B)_{(p,q)(r,s)} = \frac{1}{2}\left(\begin{vmatrix} a_{pr} & a_{ps} \\ b_{qr} & b_{qs} \end{vmatrix} + \begin{vmatrix} b_{pr} & b_{ps} \\ a_{qr} & a_{qs} \end{vmatrix} \right). \tag{18}$$

Note that while solutions to the augmented system will include all Hopf bifurcation points, there may be other solutions corresponding to neutral saddles (which occur when there are two eigenvalues that are real additive inverses). To identify and screen out neutral saddles, we compute the eigenvalues of the Jacobian at each solution of the augmented equation system. If the Hopf bifurcation occurs in an independent two-variable subset of state space, this is referred to as a planar Hopf bifurcation. In general, a Hopf bifurcation corresponds to the appearance or disappearance of a limit cycle (stable or unstable) around the equilibrium state (Seydel, 1988). Frequently this corresponds to a change in the stability of the equilibrium state. However, for systems with more than two state variables, this is not always the case, depending on the sign of the real part of other eigenvalues.

The two types of codimension-two bifurcations of interest (double-fold and fold-Hopf) can both be located by using the same augmenting functions as introduced above. When an equilibrium undergoes a double-fold bifurcation, its Jacobian has two zero eigenvalues. When an equilibrium undergoes a fold-Hopf bifurcation, its Jacobian has one eigenvalue that is zero and a pair of purely imaginary complex conjugate eigenvalues. Thus, the determinant of the Jacobian will be zero in both a double-fold and a fold-Hopf bifurcation, because in both cases there is at least one eigenvalue that is zero. Furthermore, in both cases, there is a pair of eigenvalues that will sum to zero, and so the determinant of the bialternate product $2J \odot I$ will be zero. Thus, to locate a double-fold or a fold-Hopf codimension-two bifurcation of equilibrium, the equilibrium condition can be augmented with the two additional equations $\det[J(\boldsymbol{x}, \alpha, \beta)] = 0$ and $\det[2J(\boldsymbol{x}, \alpha, \beta) \odot I] = 0$ and two additional variables (free parameters) α and β. This gives the augmented equation system

$$\frac{d\boldsymbol{x}}{dt} = \boldsymbol{f}(\boldsymbol{x}, \alpha, \beta) = 0 \tag{19}$$

$$\det[J(\boldsymbol{x}, \alpha, \beta)] = 0. \tag{20}$$

$$\det[2J(\boldsymbol{x}, \alpha, \beta) \odot I] = 0. \tag{21}$$

The augmented system is then solved to find the codimension-two bifurcations of interest, along with the corresponding values of α and β. Once found, we determine the eigenvalues of the Jacobian at each solution. This allows the solutions to be screened for neutral saddles, and to be sorted and classified by type. Codimension-two bifurcations are often of interest since they may serve as "organizing centers" for a two-parameter bifurcation diagram.

Whether one is looking for equilibrium states as discussed in Section 2.4, or the bifurcations of equilibria discussed above, there is a system of nonlinear equations to be solved that may have multiple solutions, or no solutions, and the number of solutions may be unknown *a priori*. Typically these equation systems are solved using a continuation-based strategy (Kuznetsov and Rinaldi, 1996; Kuznetsov, 1998; Kooi and Kooijman, 2000). In general, however, continuation methods are initialization dependent, and so provide no guarantee that all equilibrium states or bifurcations of equilibria will be found. Bifurcation diagrams can also be generated by using a grid-based approach in which a grid is established in the two-variable parameter space and the number and stability of equilibrium states is computed at each grid point (Fussmann et al., 2000). The resulting information can provide the approximate location of the bifurcation curves on the diagram, but does not give their exact location. A computational method is needed that is capable of finding, with certainty, *all* the solutions of the nonlinear equation systems that characterize equilibrium states and their bifurcations. We describe here an interval-Newton method for this purpose.

3 Computational Method

In this section, a brief introduction to interval mathematics is given, followed by a summary of the interval-based computational method used to solve the equation systems formulated above.

A real interval X is defined as the set of real numbers between (and including) given upper and lower bounds. That is, $X = [\underline{X}, \overline{X}] = \{x \in \Re \mid \underline{X} \leq x \leq \overline{X}\}$. Here an underline is used to indicate the lower bound of an interval while an overline is used to indicate the upper bound. An interval vector $\boldsymbol{X} = (X_1, X_2, \ldots, X_n)^T$ has n interval components, and can be interpreted geometrically as an n-dimensional rectangular polytope or "box". Similarly, an $n \times m$ interval matrix A has interval elements A_{ij}, $i = 1, 2, \ldots, n$ and $j = 1, 2, \ldots, m$. Note that in this section, uppercase quantities are intervals and lower case quantities, or uppercase quantities with an underline or overline, are real numbers.

Interval arithmetic is an extension of real arithmetic. For an elementary real arithmetic operation op $\in \{+, -, \times, \div\}$ the corresponding interval operations on intervals $X = [\underline{X}, \overline{X}]$ and $Y = [\underline{Y}, \overline{Y}]$ are defined as

$$X \text{ op } Y = \{x \text{ op } y \mid x \in X,\ y \in Y\}. \tag{22}$$

That is, the result of an interval arithmetic operation on X and Y is an interval containing all possible results of performing the operation using any number contained in X and any number contained in Y. In terms of the endpoints of X and Y,

$$X + Y = \left[\underline{X} + \underline{Y}, \overline{X} + \overline{Y}\right], \tag{23}$$

$$X - Y = \left[\underline{X} - \overline{Y}, \overline{X} - \underline{Y}\right], \tag{24}$$

$$X \times Y = \left[\min\left(\underline{X}\underline{Y}, \underline{X}\overline{Y}, \overline{X}\underline{Y}, \overline{X}\overline{Y}\right), \max\left(\underline{X}\underline{Y}, \underline{X}\overline{Y}, \overline{X}\underline{Y}, \overline{X}\overline{Y}\right)\right], \tag{25}$$

$$X \div Y = \left[\underline{X}, \overline{X}\right] \times \left[1/\overline{Y}, 1/\underline{Y}\right], \text{ where } 0 \notin \left[\underline{Y}, \overline{Y}\right]. \tag{26}$$

If $0 \in \left[\underline{Y}, \overline{Y}\right]$, the division of the two intervals X and Y can be defined using an extended interval arithmetic in which the result may not be an interval but a union of two disjoint intervals (Kearfott, 1996). Interval extensions of the elementary functions (sin, cos, tan, exp, log, etc.) can also be developed, since they can be represented as series expansions using the elementary arithmetic operations given above.

When interval arithmetic computations are performed using a computer, rounding errors must be dealt with in order to insure that the result is a rigorous enclosure. Since computers can only represent a finite set of real numbers (machine numbers), the results of floating-point arithmetic operations to compute the endpoints of an interval must be determined using a directed (outward) rounding. That is, the lower endpoint is rounded down, ideally to the largest machine number less than or equal to the lower bound, and the upper endpoint is rounded up, ideally to the smallest machine number greater than or equal to the upper bound. In this way, through the use of interval arithmetic, as opposed to floating-point arithmetic, any potential rounding error problems are avoided. Several good introductions to interval analysis, as well as interval arithmetic and other aspects of computing with intervals, are available (Neumaier, 1990; Kearfott, 1996; Jaulin et al., 2001; Hansen and Walster, 2004). Implementations of interval arithmetic and elementary functions are also readily available, and recent compilers from Sun Microsystems directly support interval arithmetic and an interval data type.

In general, for an arbitrary function $\boldsymbol{f}(\boldsymbol{x})$, the *interval extension* $\boldsymbol{F}(\boldsymbol{X})$ encloses all values of $\boldsymbol{f}(\boldsymbol{x})$ for $\boldsymbol{x} \in \boldsymbol{X}$. That is, the interval extension encloses the *range* of $\boldsymbol{f}(\boldsymbol{x})$ over $\boldsymbol{X}$. Interval extensions are most often computed by substituting the given interval $\boldsymbol{X}$ into the function $\boldsymbol{f}(\boldsymbol{x})$ and then evaluating the function using interval arithmetic. This is called the "natural" interval extension, and it may be wider than the actual range of function values, though it always includes the actual range. For example, the natural interval extension of $f(x) = x/(x-1)$ over the interval $X = [2, 3]$ is $F([2, 3]) = [2, 3]/([2, 3] - 1) = [2, 3]/[1, 2] = [1, 3]$, while the true function range over this interval is $[1.5, 2]$. This overestimation of the function range is due to the "dependency" problem, which may arise when a variable occurs more than once in a function expression. While a variable may take on any value within its interval, it must take on the *same* value each time it occurs in an expression. However, this type of dependency is not recognized when the natural interval extension is computed. In effect, when the natural interval extension is used, the range computed for the function is the range that would occur if each instance of a particular variable were allowed to take on a different value in its interval range. For the case in which $f(x)$ is a single-use expression, that is, an expression in which each variable occurs only once, interval arithmetic will always yield the true function range. For example, rearrangement of the function expression used above gives $f(x) = x/(x-1) = 1 + 1/(x-1)$, and now $F([2, 3]) = 1 + 1/([2, 3] - 1) = 1 + 1/[1, 2] = 1 + [0.5, 1] = [1.5, 2]$, the true range. For cases in which such rearrangements are not possible, there are a variety of other approaches that can be used to try to tighten interval extensions (Neumaier, 1990; Kearfott, 1996; Hansen and Walster, 2004).

Of particular interest here is the interval-Newton technique for solving nonlinear equation systems. Consider an $n \times n$ nonlinear equation system $\boldsymbol{f}(\boldsymbol{x}) = \boldsymbol{0}$

with a finite number of real roots in some initial interval $\boldsymbol{X}^{(0)}$. This initial interval can be chosen to be sufficiently large to enclose all physically feasible behavior. The interval-Newton method is applied to a sequence of subintervals of the initial interval $\boldsymbol{X}^{(0)}$; as will be seen below, these subintervals arise in a bisection process. For a subinterval $\boldsymbol{X}^{(k)}$ in the sequence, the first step is the *function range test*. An interval extension $\boldsymbol{F}(\boldsymbol{X}^{(k)})$ of the function $\boldsymbol{f}(\boldsymbol{x})$ is calculated, which provides upper and lower bounds on the range of values of $\boldsymbol{f}(\boldsymbol{x})$ in $\boldsymbol{X}^{(k)}$. If there is any component of the interval extension $\boldsymbol{F}(\boldsymbol{X}^{(k)})$ that does not include zero, then this subinterval can be discarded, since the range of $\boldsymbol{f}(\boldsymbol{x})$ does not include zero over this subinterval, meaning that it cannot contain a solution to $\boldsymbol{f}(\boldsymbol{x}) = \boldsymbol{0}$. Additional tools, such as constraint propagation (e.g., Jaulin et al., 2001) or Taylor models (e.g., Makino and Berz, 2003), may also be applied at this point in order to reduce the size of $\boldsymbol{X}^{(k)}$ or eliminate it.

If it has not been eliminated, the testing of $\boldsymbol{X}^{(k)}$ continues with the *interval-Newton test*, which involves solving the linear interval equation system

$$F'(\boldsymbol{X}^{(k)}) \left[\boldsymbol{N}^{(k)} - \boldsymbol{x}^{(k)}\right] = -\boldsymbol{f}(\boldsymbol{x}^{(k)}). \qquad (27)$$

Eq. (27) is solved for a new interval $\boldsymbol{N}^{(k)}$, where $F'(\boldsymbol{X}^{(k)})$ is an interval extension of the Jacobian of $\boldsymbol{f}(\boldsymbol{x})$ over the interval $\boldsymbol{X}^{(k)}$, and $\boldsymbol{x}^{(k)}$ is an arbitrary point in $\boldsymbol{X}^{(k)}$. It can be shown (Moore, 1966) that any root contained in $\boldsymbol{X}^{(k)}$ is also contained in the "image" $\boldsymbol{N}^{(k)}$. This implies that when the intersection $\boldsymbol{X}^{(k)} \cap \boldsymbol{N}^{(k)}$ is empty, then no root exists in $\boldsymbol{X}^{(k)}$, and also suggests the iteration scheme $\boldsymbol{X}^{(k+1)} = \boldsymbol{X}^{(k)} \cap \boldsymbol{N}^{(k)}$. In addition, if $\boldsymbol{N}^{(k)} \subset \boldsymbol{X}^{(k)}$, it can been shown (Kearfott, 1996) that there is a *unique* root contained in $\boldsymbol{X}^{(k)}$ and thus in $\boldsymbol{N}^{(k)}$. Thus, after computation of $\boldsymbol{N}^{(k)}$, there are three possible outcomes: 1. $\boldsymbol{X}^{(k)} \cap \boldsymbol{N}^{(k)} = \emptyset$, meaning the current interval $\boldsymbol{X}^{(k)}$ is shown to contain no root, so it can be discarded; 2. $\boldsymbol{N}^{(k)} \subset \boldsymbol{X}^{(k)}$, meaning the current interval $\boldsymbol{X}^{(k)}$ is shown to contain a unique root, so it need not be further tested; 3. Neither of the above, but a new interval $\boldsymbol{X}^{(k+1)} = \boldsymbol{X}^{(k)} \cap \boldsymbol{N}^{(k)}$ can be generated. In the last case, if there has been a significant reduction in the size of the interval, then the interval-Newton test can be reapplied. Otherwise, the interval $\boldsymbol{X}^{(k+1)}$ is bisected, and the resulting two subintervals are added to the sequence of subintervals to be tested. If an interval containing a unique root has been identified, then this root can be tightly enclosed by continuing the interval-Newton iteration, which will converge quadratically to a desired tolerance.

This approach is referred to as an interval-Newton/generalized-bisection (IN/GB) method. At termination, when the subintervals in the sequence have all been tested, either all the real roots of $\boldsymbol{f}(\boldsymbol{x}) = \boldsymbol{0}$ have been tightly enclosed or it is determined rigorously that no roots exist. An important feature of this approach is that, unlike standard methods for nonlinear equation solving that require a *point* initialization, the IN/GB method requires only an initial *interval*, and this interval can cover the entire state and parameter space of interest. Thus, interval-Newton methods essentially need no initialization. It should be emphasized that the interval-Newton approach is *not* equivalent to simply implementing the routine "point" Newton method in interval arithmetic. For a more thorough treatment of interval-Newton methods, there are several good sources available (Neumaier, 1990; Kearfott, 1996; Hansen and Walster, 2004). For additional details on the basic IN/GB algorithm used here, see Schnepper and Stadtherr (1996). Several enhancements of this basic algorithm are also employed, namely the hybrid preconditioning approach and real-point selection strategy described by Gau and Stadtherr (2002).

Using the interval method described in this section, it is possible to determine *all* solutions to a nonlinear equation system within a desired search interval, or to show that no such solutions exist. This can be done not only with *mathematical certainty*, but also with *computational certainty*, since the use of interval arithmetic with outward rounding eliminates any possible rounding error issues. This guarantee, together with the lack of need for initialization, are significant advantages over traditional techniques for the location of equilibrium states and bifurcations. In the next section, we apply the IN/GB approach to the analysis and comparison of the example food chain models described above.

4 Results and Discussion

In this section, we apply the computational method described above to compute bifurcation diagrams for the three example models of interest, and use these results to compare the models. It should be noted that, since these are relatively simple models, it is possible to perform some of these computations analytically. However, since this may not be possible for more complex models, all the results presented below were computed numerically using the IN/GB technique, without any analytical short cuts.

4.1 Rosenzweig-MacArthur Model

Since this model, described above in Section 2.1, is relatively simple and has been widely studied both analytically and numerically, it provides a good "proof of concept" problem for testing the feasibility of the interval-based method described in Section 3 for determining equilibrium states and bifurcations of equilibria in food chain models. Following Gragnani et al. (1998), the

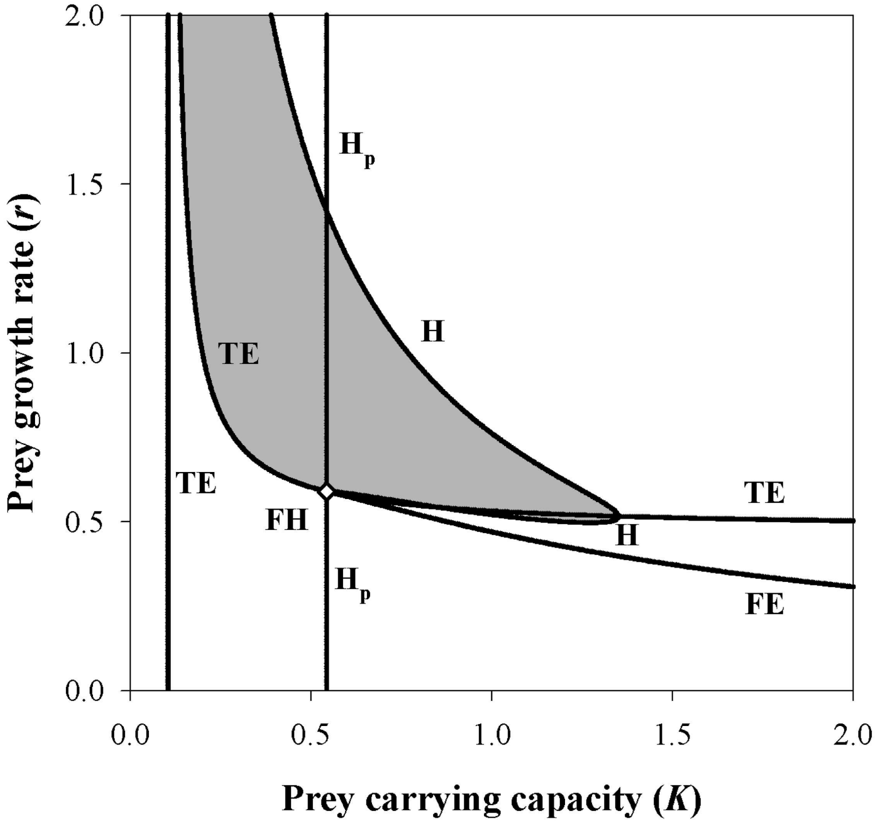

Fig. 1. Bifurcation of equilibrium diagram of prey carrying capacity (K) versus prey growth rate (r) for the Rosenzweig-MacArthur model. TE: Transcritical of equilibrium; FE: Fold of equilibrium; H: Hopf; $\mathrm{H_p}$: Planar Hopf; FH: Fold-Hopf codimension-two. Region of stable coexistence shaded in grey.

parameters used are set to $a_2 = 5/3$, $b_2 = 1/3$, $e_2 = 1$, $d_2 = 0.4$, $a_3 = 0.05$, $b_3 = 0.5$, $e_3 = 1$, $d_3 = 0.01$. Using the IN/GB equation-solving method described in Section 3, together with the plotting procedure described below, a bifurcation diagram with the prey growth rate, r, and the prey carrying capacity, K, as the free parameters was determined. This diagram is given in Fig. 1.

Codimension-one bifurcation curves were computed by solving the appropriate augmented systems, namely Eqs. (14-15) for fold and transcritical bifurcations and Eqs. (16-17) for Hopf bifurcations. The diagram shown in Fig 1 was generated by first fixing r at many (400) closely spaced values over the interval [0,2] and determining the value(s) of K and $\boldsymbol{x}$ at which bifurcations occur. There may be some values of r for which one of the augmented systems has an infinite number of solutions for K. For example, in Fig. 1, the left-most transcritical bifurcation is a vertical line. This case cannot be handled directly by the IN/GB technique, or could be missed by the stepping in r. Thus, to ensure that all bifurcations are found, it is necessary to also scan in the K direction. That is, IN/GB was used to solve the appropriate augmented systems for r and $\boldsymbol{x}$ for many (400) closely spaced values of K over the interval [0,2]. Codimension-two bifurcations were located by using IN/GB to solve the augmented system given by Eqs. (19-21) for K, r, and $\boldsymbol{x}$. The bifurcation diagram (Fig. 1) computed using the interval method is consistent with the known K versus r bifurcation diagram given by Gragnani et al. (1998), thus confirming the utility and accuracy of this method for determining bifurcation of equilibria diagrams. Such diagrams can be very easily and automatically generated using the IN/GB approach, with certainty that all bifurcation curves have been found.

Another useful type of diagram in nonlinear dynamics is the solution branch diagram (or one-parameter bifurcation diagram). This type of diagram shows how the steady-state values and stability of the state variables change as a single model parameter is varied. These diagrams are also very easily generated using the interval method. For example, Fig. 2 shows how the equilibrium states change as the prey carrying capacity, K, is varied from 0 to 2, while the prey growth rate, r, is held constant at a value of 0.5. This diagram was computed by using IN/GB to solve the nonlinear equation system given by Eq. (12). This system was solved for many (2000) closely spaced values of K. In Fig. 2, and in subsequent solution branch diagrams, thin lines represent unstable equilibria while thick lines represent stable equilibria.

In the solution branch diagram, one can observe several bifurcations of equilibria as K is increased. This can also be seen by following a horizontal line across Fig. 1 at a value of $r = 0.5$. Moving to the right along this line, five bifurcations are encountered, namely (and in order) TE, $\mathrm{H_p}$, FE, H, H (the rightmost TE is not crossed at $r = 0.5$). The first bifurcation to occur is a transcritical bifurcation ($K \approx 0.105$), in which a stable prey-only state collides with a prey-predator state which becomes feasible at the bifurcation. These states exchange stability. The predator biomass then begins to increase while the prey biomass remains constant. The next bifurcation that is observed is a planar Hopf bifurcation ($K \approx 0.544$). Since this bifurcation occurs at an r value *below* the fold-Hopf codimension-two bifurcation, this planar Hopf bifurcation does result in a change in stability in the model. *Above* the fold-Hopf point, the prey-predator state is feasible but is unstable due to the sign of the third eigenvalue, and thus the planar Hopf bifurcation does not result in a change of stability. The next bifurcation to occur is a fold bifurcation ($K \approx 0.872$) where two unstable coexisting (prey-predator-superpredator) states become feasible. The next two bifurcations to occur are both Hopf bifurcations ($K \approx 1.186$ and $K \approx 1.329$). In the first Hopf bifurcation, one of the coexisting states becomes stable, and the same state become unstable in the subsequent bifurcation. In the narrow interval of K that produces a stable, coexisting steady state, increasing the prey carrying capacity increases the biomass of the superpredator.

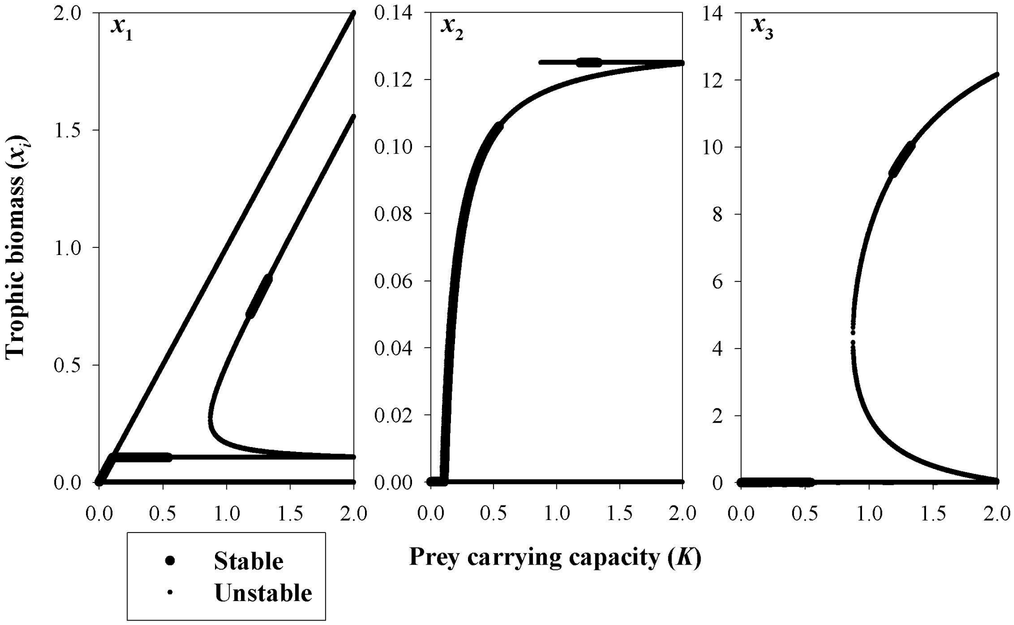

Fig. 2. Solution branch diagrams illustrating the change in equilibrium states (species biomass) with change in the prey carrying capacity (K) for the Rosenzweig-MacArthur model. From left to right: prey, predator, and superpredator biomasses. $r = 0.5$ for all three plots.

Thus, by feeding the bottom level of the food chain, the abundance of the top level can be increased. However, this strategy only works to a point, and then the system becomes unstable. This phenomena is well known in the field of theoretical ecology as the "paradox of enrichment" (Abrams and Roth, 1994).

Regions in a bifurcation diagram such as Fig. 1 can be characterized by using solution branch diagrams such as Fig. 2, or by directly computing the number and stability of equilibrium states for a point in a given region. Often the region of particular interest may be that corresponding to the values of r and K that produce a stable, coexisting steady-state (all species present). This region is shown by the shaded area in Fig. 1. Within this region, as the prey growth rate r increases, the resources required by the prey (represented by the prey carrying capacity K) to support a stable, coexisting state decreases. However, at the same time, the system becomes more sensitive to enrichment, and the amount of enrichment necessary to destabilize the system also decreases. This phenomena makes sense mathematically when one considers that both the prey growth rate, r, and the prey carrying capacity, K, control increases in the prey population. Therefore, increasing either r or K can have the effect of destabilizing the system. However, only the parameter K describes enrichment of resources in the system.

Using the techniques described in this paper, bifurcation diagrams for other

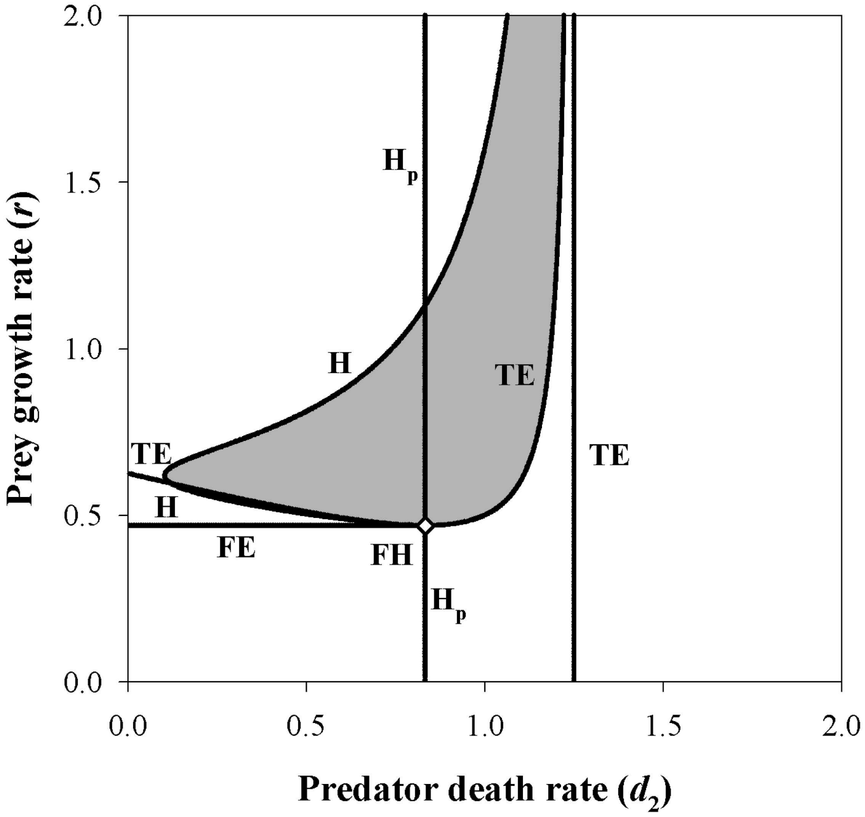

Fig. 3. Bifurcation of equilibrium diagram of predator death rate (d_2) versus prey growth rate (r) for the Rosenzweig-MacArthur model with $K = 1.0$ TE: Transcritical of equilibrium; FE: Fold of equilibrium; H: Hopf; $\mathrm{H_p}$: Planar Hopf; FH: Fold-Hopf codimension-two. Region of stable coexistence shaded in grey.

model parameters can be generated with ease. Similarly, it is also easy to determine bifurcation diagrams for variations of the Rosenzweig-MacArthur model in which other predator response functions (e.g., sigmoidal or Holling type III) are used. Several such bifurcation diagrams have been computed using the interval method by Gwaltney et al. (2004). One of these will be discussed here so that comparisons can be made with the other models used as examples. This is the bifurcation diagram for the Rosenzweig-MacArthur model with the prey growth rate r and predator death rate d_2 as bifurcation parameters, and $K = 1$. This diagram was determined using the IN/GB approach and is shown in Fig. 3.

Using solution branch diagrams to characterize the regions in Fig. 3 shows that the rightmost transcritical bifurcation, which is a vertical line, forms the boundary between a stable prey-predator system (on the left) and a stable prey-only system (on the right). Moving to the left, the next transcritical bifurcation curve intersects a codimension-two fold-Hopf point. At d_2 values to the right of the fold-Hopf point, this transcritical bifurcation is the boundary between the stable coexisting steady state and the stable prey-predator state. After the transcritical line intersects the fold-Hopf point, three bifurcation curves are formed. These are a fold bifurcation, a transcritical bifurcation, and a Hopf bifurcation. The fold bifurcation is a horizontal line ($r \approx 0.46875$) that originates at the fold-Hopf bifurcation. When increasing r and crossing this fold bifurcation, two coexisting states form. Whether the transcritical bifurcation or the Hopf bifurcation is crossed next depends on the value of d_2. Crossing the transcritical bifurcation results in one of the two coexisting states becoming infeasible. The state that becomes infeasible is also unstable. The other state formed in the fold bifurcation becomes stable in the region above and to the right of the Hopf bifurcation emanating from the fold-Hopf point. With this knowledge, we have an understanding of the region of coexisting stability in the d_2 versus r parameter space. This region is shown by the shaded area in Fig. 3. The shape of the region of coexisting stability indicates that as the predator death rate, d_2, increases, the minimum prey growth rate necessary to support a stable system will first decrease up to the codimension-two fold-Hopf point, then increase. Furthermore, at larger prey growth rates, the system will tolerate higher predator death rates before the coexisting state becomes infeasible. Finally, it is clear that there is an optimal prey growth rate that will support the widest range of predator death rates.

4.2 Canale's Chemostat Model

The second food chain model used as an example here is Canale's chemostat model, as described in Section 2.2. Following Gragnani et al. (1998), the parameters used are set to $a_1 = 1.25$, $b_1 = 8$, $e_1 = 0.4$, $d_1 = 0.01$, $\varepsilon_1 = 1$, $a_2 = 0.33$, $b_2 = 9$, $e_2 = 0.6$, $d_2 = 0.001$, $\varepsilon_2 = 0.8$, $a_3 = 0.021$, $b_3 = 15.19$, $e_3 = 0.9$, $d_3 = 0.0001$, $\varepsilon_3 = 0.1$. A bifurcation diagram with the inflow rate, D, and the concentration of the nutrient in the inflow, x_n, as the free parameters was then computed using the IN/GB method. This diagram is shown in Fig. 4.

The codimension-one bifurcation curves were computed by solving the appropriate equation systems (see Section 2.5), first fixing x_n at many (400) closely spaced values over the interval [0,400] and determining the value(s) of D and $\boldsymbol{x}$ at which bifurcations occur, and then fixing D at many (700) closely spaced values over the interval [0,0.14] and determining the value(s) of x_n and $\boldsymbol{x}$ at which bifurcations occur. A single codimension-two (fold-Hopf) bifurcation was located by solving the appropriate augmented system for x_n, D, and $\boldsymbol{x}$.

Fig. 4 captures all bifurcations of equilibria shown in the D vs. x_n bifurcation diagram presented by Gragnani et al. (1998). However, Fig. 4 also shows other

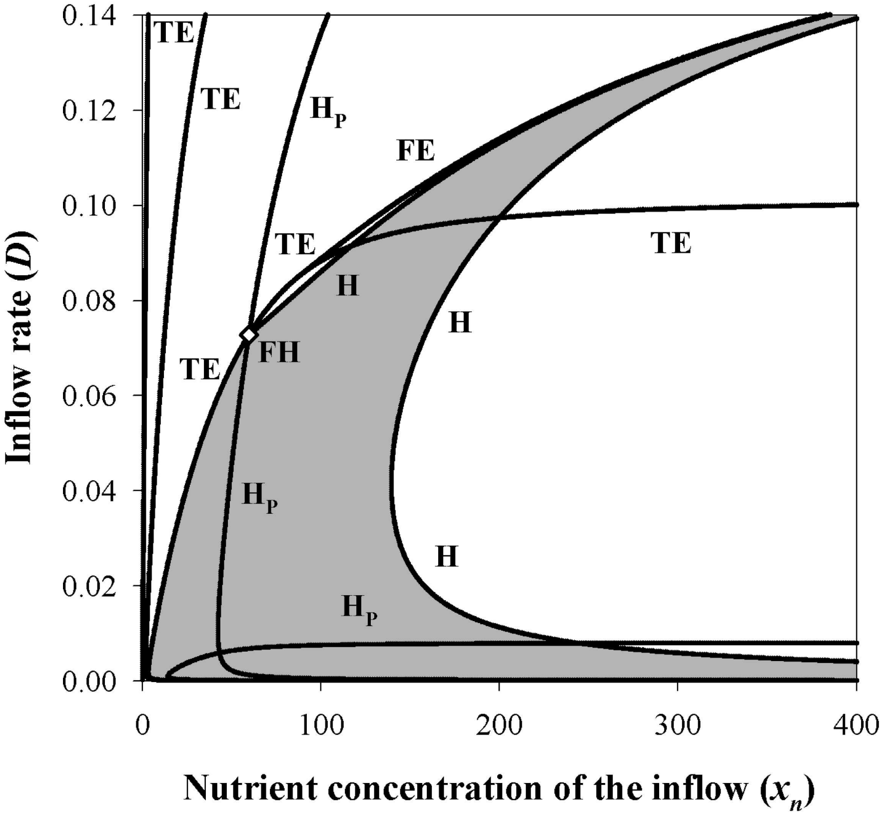

Fig. 4. Bifurcation of equilibrium diagram of nutrient inflow concentration (x_n) versus inflow rate (D) for Canale's chemostat model. TE: Transcritical of equilibrium; FE: Fold of equilibrium; H: Hopf; $\mathrm{H_p}$: Planar Hopf; FH: Fold- Hopf codimension-two. Region of stable coexistence shaded in grey.

bifurcation curves that do not appear in Gragnani *et al.*'s diagram. First, there is a transcritical bifurcation curve very near the D axis (the leftmost TE in Fig. 4) that is not given by Gragnani *et al.* At this bifurcation, a stable nutrient-only equilibrium state collides with an infeasible nutrient-prey equilibrium state; the nutrient-prey state becomes feasible and exchanges stability with the nutrient-only state. Second, there is a planar Hopf bifurcation curve near the x_n axis (lowest $\mathrm{H_p}$ in Fig. 4) that is not shown by Gragnani *et al.* (we have also computed other planar Hopf bifurcations curves very near the x_n axis, but these are not visible in Fig. 4 due to the scale used). For all of these $\mathrm{H_p}$ bifurcations, the stability change occurs only in a two-variable subspace, with the stability of the overall system remaining unchanged (unstable); this is also the case for the lower portion (beneath the fold-Hopf point) of the planar Hopf curve that intersects the fold-Hopf point, which appears both in Fig. 4 and in Gragnani *et al.*'s diagram. Whether the planar Hopf curves omitted from Gragnani et al.'s diagram were actually not found, or were omitted simply because they were not considered interesting, is not clear. What is important

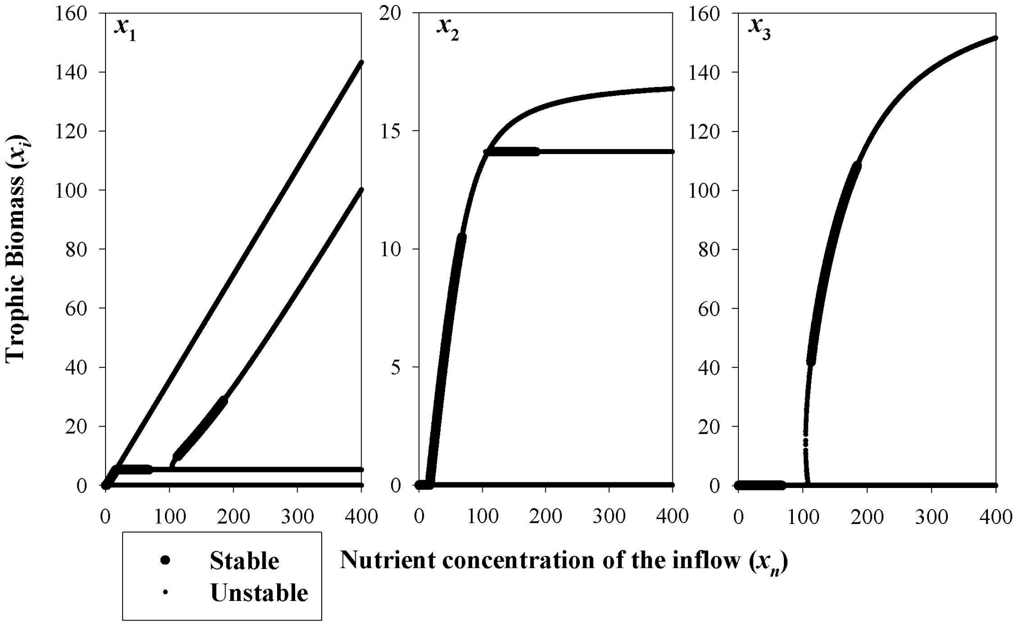

Fig. 5. Solution branch diagrams illustrating the change in equilibrium states (species biomass) with change in the nutrient concentration of the inflow (x_n) for Canale's chemostat model. From left to right: prey, predator, and superpredator biomasses. $D = 0.09$ for all three plots.

here is that, by using the IN/GB method, we can say with complete confidence that we have in fact found all of the bifurcations curves of interest.

Fig. 5 tracks the behavior of the equilibrium states as x_n is increased from 0 to 400 along the horizontal line $D = 0.09$ in Fig. 4. Moving to the right along this line, seven bifurcations are encountered, namely (and in order) TE, TE, H_p, FE, TE, H, H. The first TE is not clearly visible in Fig. 5 due to the scale used. The sixth and seventh bifurcations, both Hopf, are of particular interest here. The sixth bifurcation ($x_n \approx 112.5$) results in the first stable, coexisting steady-state (all three species present). But at the seventh bifurcation ($x_n \approx 184.5$), this state becomes unstable. However, within this region of stability increasing the inflow nutrient concentration, x_n, enriches the food chain and increases the stable population of the top predator, but only to a point. This again illustrates the "paradox of enrichment" in that beyond the second Hopf bifurcation the system becomes unstable and the populations may experience "boom and bust" cycles. This behavior is very similar to the behavior observed in Fig. 2, which indicates that, while the Rosenzweig-MacArthur model does not explicitly account for resources, it can produce similar behavior when compared to a resource-based model, such as Canale's model.

Using solution branch diagrams like Fig. 5 we can characterize the regions in

Fig. 4 and identify the bounds on the region of x_n and D that corresponds to a stable, coexisting steady-state. This region is shown by the shaded area in Fig. 4. As indicated in Fig. 4, as the inflow rate, D, increases, the minimum inflow nutrient concentration, x_n, required to support a coexisting steady-state also increases. This behavior is intuitive because, as the inflow rate increases, more nutrient and organisms are washed out of the system, resulting in the need for a higher nutrient inflow concentration, x_n, to support the minimum biomasses of prey and predators necessary for survival of the predators and superpredators, respectively.

The maximum x_n boundary for the region supporting a stable, coexisting steady state of all three species is the rightmost Hopf bifurcation curve. At x_n values to the of right this curve, the system is over-enriched and loses stability. One can thus see from Fig. 4 that at relatively low inflow rates ($D \lessapprox 0.0414$), increasing D causes the maximum x_n allowable for a stable coexisting state to decrease. This can be explained by recognizing that at very low values of the inflow rate, D, increasing the inflow rate has the predominant effect of increasing the addition of nutrients to the system, thereby leading to over-enrichment and decreasing the inflow nutrient concentration at which the rightmost Hopf bifurcation occurs in Fig. 4. However, at values of $D \gtrapprox 0.0414$, increasing the inflow rate causes the effects of washout to become more pronounced, and larger values of x_n are allowable because of the high removal rate of both biomass and system nutrient.

Various authors have utilized bifurcation diagrams to make comparisons between different food chain model formulations. Kooi et al. (1997b, 1998) compared several different formulations of chemostat-based food chain models. These authors used model formalisms to compare simple formulations with two state variables, while models with three or four state variables were compared using bifurcation diagrams. These latter models are similar in formulation to the Rosenzweig-MacArthur model and Canale's chemostat model, as studied here and by Gragnani et al. (1998), however a different set of parameters was used. Kooi et al. (1997b, 1998) concluded that chemostat-based models exhibited fundamentally different behavior than models with prey that grow according to the logistic growth function. On the other hand, Gragnani et al. (1998) compared the Rosenzweig-MacArthur model (logistic prey) with Canale's chemostat model under conditions of enrichment, and concluded that the two models produce the same dynamics when a key parameter is varied. That is, the dynamics observed when K was varied in the Rosenzweig-MacArthur model were equivalent to those in Canale's model when x_n was varied. Since Kooi et al. (1997b, 1998) and Gragnani et al. (1998) studied systems under much different conditions (model parameters), these conclusions are not necessarily in conflict.

In this work, we can compare the shaded region in Fig. 4 with the region producing a stable, coexisting steady state for the Rosenzweig-MacArthur model (Fig. 1). This comparison indicates that these regions are dissimilar. That is, the behavior observed when changing both r and K is not equivalent to the behavior observed when changing both D and x_n. This is due to inconsistencies between the parameters compared in these models. The prey growth rate r in the Rosenzweig-MacArthur model is not equivalent to the system inflow rate D in Canale's model. Thus, the use of a different parameter set in the analysis of Canale's chemostat model may be appropriate for making comparisons of behavior with the Rosenzweig-MacArthur model. Since the Rosenzweig-MacArthur model does not explicitly account for resources or for washout, there is no parameter in that model that is equivalent to D. However, in Canales model, the prey species grows at a maximum rate of $e_1 a_1$; thus changing the maximum nutrient consumption rate by the prey, a_1, should have a similar effect to changing the prey growth rate r in the Rosenzweig-MacArthur model. Using IN/GB and the techniques described above, it is a relatively easy matter to generate a bifurcation diagram in the x_n vs. a_1 parameter space. This diagram appears as Fig. 6. Since Fig. 4 and Fig. 6 share a common parameter (x_n), the figures should intersect in a three-dimensional parameter space. In fact, the bifurcations that occur along the lines $D = 0.07$ in Fig. 4 and $a_1 = 1.25$ in Fig. 6 occur in the same order and at the same values. This fact makes classification of some of the bifurcation lines much easier.

Comparison of Fig. 6 for Canale's model and Fig. 1 for the Rosenzweig-MacArthur model shows clear similarities. There are differences, including an additional transcritical bifurcation (which must exist due to the extra state variable x_0) and the general shape of the bifurcation curves. However, the order in which one crosses these curves, whether moving from left to right, or top to bottom, is the same in both diagrams. The region in Fig. 6 in which there is a stable, coexisting steady state is shown by the shaded area. This region is very similar in shape to the region of steady, stable coexistence in Fig. 1. The behavior observed is very similar to the behavior discussed in Section 4.1 in that, as a_1 increases, the amount of food required by the prey, x_n, to support a stable, coexisting state decreases. However, at the same time, increasing a_1 also causes the system to become more sensitive to enrichment, and thus the amount of enrichment necessary to destabilize the system also decreases. The most noticeable differences between Fig. 6 and Fig. 1 pertain mainly to lines controlling the feasibility and stability of trophic subsystems in the models, such as the nutrient-prey-predator system in Canale's model and the prey-predator system in the Rosenzweig-MacArthur model. The qualitative behavior in the region of stable coexistence is very similar in both models.

We can make a similar comparison by using the IN/GB method to generate an a_1 versus d_2 bifurcation diagram for Canale's model. This diagram,

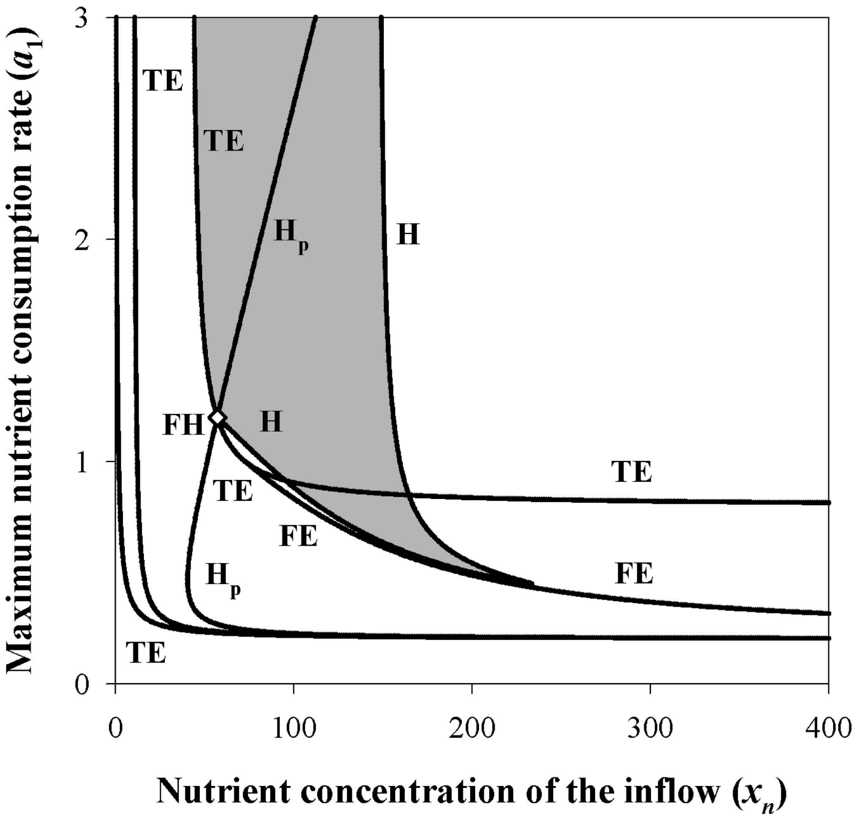

Fig. 6. Bifurcation of equilibrium diagram of nutrient inflow concentration (x_n) versus maximum nutrient consumption rate by the prey (a_1) for Canale's chemostat model with $D = 0.07$. TE: Transcritical of equilibrium; FE: Fold of equilibrium; H: Hopf; $\mathrm{H_p}$: Planar Hopf; FH: Fold-Hopf codimension-two. Region of stable coexistence shaded in grey.

given in Fig. 7, can be compared to the to the r versus d_2 diagram for the Rosenzweig-MacArthur model (Fig. 3). In Fig. 7, several of the bifurcation curves lie very close together. Following a vertical line in Fig. 7 (increasing a_1) at the value of the predator death rate used by Gragnani et al. (1998) ($d_2 = 0.001$), we encounter seven bifurcations, namely (and in order): TE, TE, $\mathrm{H_p}$, FE, H, H, TE. Initially the system has only one steady-state, which is a stable nutrient-only state. At a_1 values below the horizontal transcritical bifurcation ($a_1 = 0.208$), the prey does not consume nutrient quickly enough for a nutrient-prey state to be feasible. In the first transcritical bifurcation, a nutrient-prey state forms, collides, and exchanges stability with the nutrient-only state. In the second transcritical bifurcation, a nutrient-prey-predator system becomes feasible and exchanges stability with the nutrient-prey state. Then, as the planar-Hopf bifurcation is crossed, the nutrient-prey-predator state loses stability. Due to the proximity of these three bifurcation lines at low values of the predator death rate, the transition from a condition where

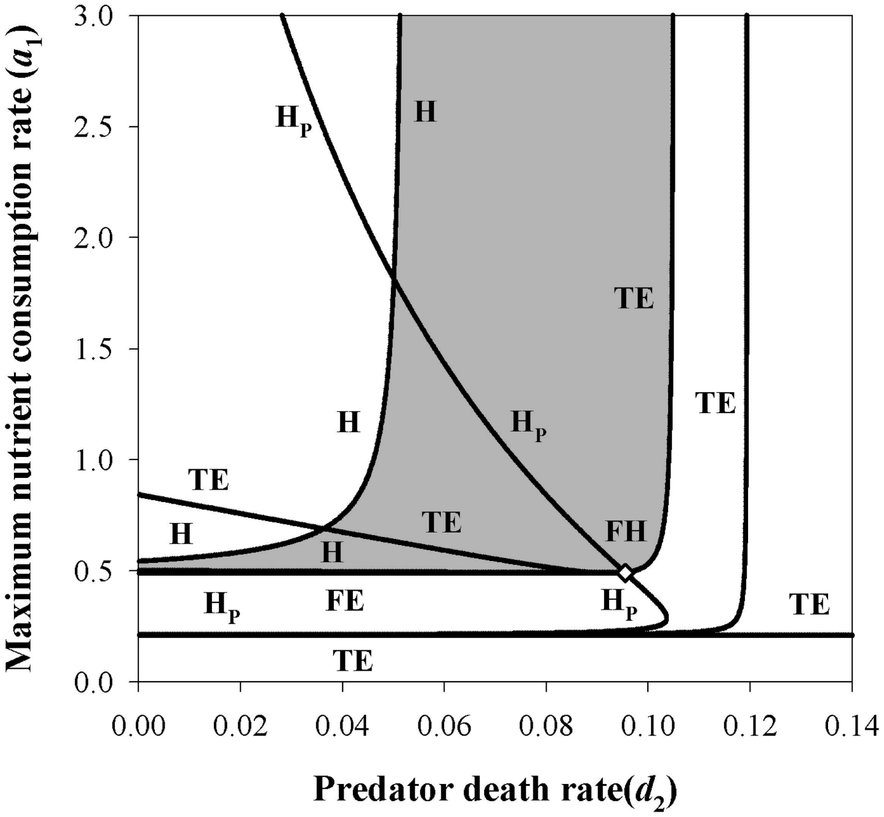

Fig. 7. Bifurcation of equilibrium diagram of predator death rate (d_2) versus maximum nutrient consumption rate by the prey (a_1) for Canale's chemostat model with $D = 0.07$ and $x_n = 200.0$. TE: Transcritical of equilibrium; FE: Fold of equilibrium; H: Hopf; $\mathrm{H_p}$: Planar Hopf; FH: Fold-Hopf codimension-two. Region of stable coexistence shaded in grey.

the only feasible state is the (stable) nutrient-only state to a condition where there are three feasible states, none of which are stable, occurs over a very small range of a_1. As the maximum nutrient consumption rate (a_1) is further increased a fold bifurcation is crossed, which causes two coexisting states to become feasible, but neither are stable. This fold bifurcation is, in fact, a horizontal line with a value of $a_1 \approx 0.487$. The behavior of this fold bifurcation is qualitatively identical to that observed in Fig. 3. The presence of a horizontal fold bifurcation marking the boundary for coexisting feasibility indicates that the prey growth rate r in the Rosenzweig-MacArthur model, and the maximum nutrient consumption rate a_1 in Canale's model are comparable parameters, and they have very similar effects on system behavior. Furthermore, it indicates that there is a minimum r or a_1 below which the prey simply cannot grow fast enough to replace losses and maintain a feasible, coexisting steady state, and that this minimum value is independent of the predator death rate d_2. The Hopf bifurcation, which originates in the fold-Hopf codimension-two bifurcation, is crossed next. When this bifurcation is crossed, one of the coexisting states becomes stable. The fold bifurcation and Hopf bifurcation occur at extremely close values of a_1, which results in the two lines being almost indistinguishable on Fig. 7. Crossing the second Hopf bifurcation (which enters the diagram on the a_1 axis) causes the stable coexisting state to become unstable. Crossing the subsequent transcritical bifurcation causes the unstable coexisting state that did not change stability due to the Hopf bifurcation to become infeasible. This transcritical bifurcation, which emanates from the fold-Hopf codimension-two point, causes the same change in system behavior as the transcritical line emanating from the fold-Hopf point in Fig. 3.

With this knowledge, we can visualize the region of coexisting feasibility and stability. This region is shown by the shaded area in Fig. 7. The transcritical bifurcation that intersects the fold-Hopf bifurcation forms the right boundary of steady, stable coexistence at predator death rate values greater than the codimension-two fold-Hopf bifurcation ($d_2 \approx 0.0955$). To the right of this transcritical bifurcation the predator death rate is too large and the superpredator population is decimated. This behavior is also identical to that observed in Fig. 3. Thus, at some point no matter how quickly the prey are able to grow and replace their losses, increasing the predator death rate will cause a stable coexisting steady-state to become infeasible. This macroscopic change occurs when the superpredator population disappears, not the predator population, even though it is the predator death rate that is increasing. While this behavior is counterintuitive, as explained in Gwaltney et al. (2004), similar behavior can also be seen in the Rosenzweig-MacArthur model.

As indicated by the shaded areas, the regions in Fig. 3 and Fig. 7 supporting a stable, coexisting steady-state are very similar in shape. The primary difference is that in Fig.7, the Hopf bifurcation line emanating from the fold-Hopf bifurcation does not reverse direction. Instead, moving to the left, it crosses the a_1 axis. Another Hopf bifurcation then enters the diagram on the a_1 axis, and this Hopf bifurcation causes the same change in stability that is caused by the Hopf bifurcation in Fig. 3 after it changes direction. Actually, if Fig. 7 were extended into the negative d_2 parameter space, we could see that the two Hopf bifurcations are actually a continuous curve that reverses direction, just like in Fig. 3. The key bifurcation lines that control the feasibility of the coexisting state are identical in behavior to those observed in Fig. 3. In general, as the maximum nutrient consumption rate by the prey, a_1, increases, the system given by Canale's Chemostat model is able to tolerate higher predator death rates before the coexisting state becomes infeasible. In Canale's model we also observe that as the maximum nutrient consumption rate by the prey increases, the minimum predator death rate necessary to support a stable coexisting state increases. This behavior matches the behavior observed in Fig. 3 for the Rosenzweig-MacArthur model.

The primary differences between Fig. 7 for Canale's model and Fig. 3 for the Rosenzweig-MacArthur model are seen in the bifurcation lines which deal with the boundaries at which the predator population becomes infeasible, and where the prey-predator subsystem changes stability. These lines are the planar Hopf bifurcation and the rightmost transcritical bifurcation in Figs. 3 and 7. An additional horizontal transcritical bifurcation is present in Fig. 7. The presence of this bifurcation is expected as it provides the boundary between the nutrient-only state and the nutrient-prey state. The fact that the line is horizontal indicates that the minimum value of a_1 necessary to support a feasible (and stable) nutrient-prey state does not depend on the predator death rate, d_2. This behavior is expected because the behavior of the nutrient-prey subsystem should not depend on any parameters not appearing in the subsystem, including the predator death rate. We will observe identical behavior in examining the algae-rotifer model, which is also explicitly accounts for resources by modeling the limiting nutrient in a chemostat.

4.3 Algae-Rotifer Model

The final food chain model used as an example here is the algae-rotifer model, as described in Section 2.3. Following Fussmann et al. (2000), the parameters used are set to $b_C = 3.3$ day^{-1}, $K_C = 4.3\,\mu$mol/liter, $b_B = 2.25$ day^{-1}, $K_B = 15\,\mu$mol/liter, $m = 0.055$ day^{-1}, $\lambda = 0.4$ day^{-1}, and $\varepsilon = 0.25$. The four state variables (N, C, R and B) are modeled in terms of nitrogen concentration (μmol/liter), with the last three then converted to numbers of organisms according to $1\,\mu$mol/liter $= 5 \times 10^4$ cells per milliliter for *Chlorella* and $1\,\mu$mol/liter $= 5$ females per milliliter for *Brachionus*. A bifurcation diagram with the inflow rate, δ, and the concentration of the nitrogen in the inflow, N_i, as the free parameters was then computed using the IN/GB method, and is given in Fig. 8.

Fussmann et al. (2000) determined a δ vs. N_i bifurcation diagram by using a grid-based approach in which a grid is established in the two-variable parameter space and the number and stability of equilibrium states is computed directly at each grid point. In comparing Fig. 8 to the diagram presented by Fussmann et al. (2000), one should note that the axes have been reversed in order to facilitate comparisons with the models previously discussed in this work. Furthermore, the diagram presented by Fussmann et al. (2000) contained a region for the coexistence of stable limit cycles, which are not examined in this work. Finally, Fig. 8 shows a transcritical bifurcation along the inflow rate (δ) axis, which does not appear in Fussmann et al. (2000). This occurs because the diagram in Fussmann et al. (2000) is limited to defining regions in which a stable, coexisting state exists (whether it is an equilibrium state or a limit cycle).

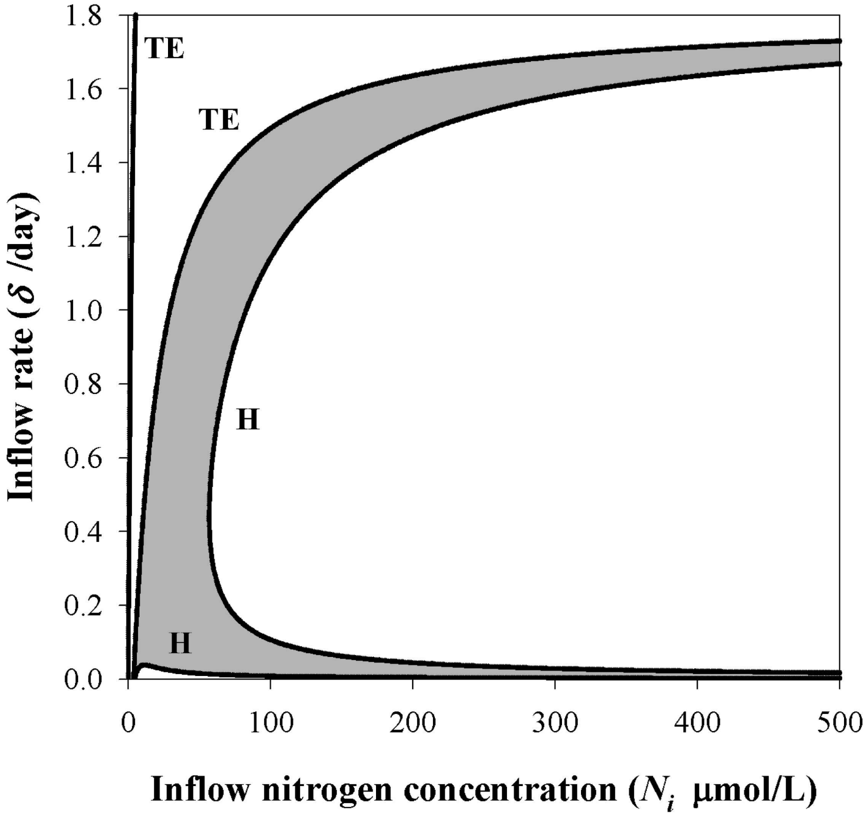

Fig. 8. Bifurcation of equilibrium diagram of inflow nitrogen concentration (N_i) versus inflow rate (δ) for the algae-rotifer model. TE: Transcritical of equilibrium; H: Hopf. Region of stable coexistence shaded in grey.

In Fig. 8, as N_i increases, in most cases three bifurcations will be crossed, and these are (from left to right) two transcritical bifurcations and a Hopf bifurcation. At values of $\delta \lessapprox 0.037$, another Hopf bifurcation will also be crossed. As the leftmost transcritical bifurcation is crossed, a stable nitrogen-algae system becomes feasible. As the second transcritical bifurcation is crossed, a stable coexisting (nitrogen-algae-rotifer) state becomes feasible (and the nitrogen-algae system becomes unstable). Finally, as the Hopf bifurcation is crossed, the stable coexisting state becomes unstable. Crossing the Hopf bifurcation near the N_i axis also causes the stable coexisting state to become unstable. At a given value of N_i, at values of δ below this Hopf bifurcation, the coexisting state is feasible, but unstable.

The region where a coexisting steady-state is both feasible and stable is shown by the shaded area in Fig. 8. When comparing Fig. 8 with Fig. 4, one may initially notice a similarity between the regions of steady, stable coexistence. However, recall that the algae-rotifer model only features two trophic levels, while Canale's model features three. Thus, the rightmost transcritical and

Hopf bifurcations in Fig. 8 are equivalent to the middle transcritical bifurcation and the planar Hopf bifurcation passing through the fold-Hopf point in Fig. 4. Even taking this into account, the behavior of the stable, coexisting state (nitrogen-algae-rotifer) in the algae-rotifer model matches the same trends observed in the nutrient-prey-predator subspace of Canale's chemostat model. There is one primary difference, that being that the lower boundary in Fig. 4 is formed by the transcritical bifurcation (which also forms the left boundary) while in Fig. 8, the lower boundary consists of a Hopf bifurcation. Despite this difference, it should be recognized that increasing the dilution rate (δ) or the nitrogen concentration in the inflow medium (N_i) has a similar effect to increasing either D or x_n on the nutrient-prey-predator state in Canale's chemostat model. Thus these models exhibit similar behavior in terms of the effects of enrichment, and the paradox of enrichment also applies to the algae-rotifer model.

In order to further compare the algae-rotifer model with both the Rosenzweig-MacArthur model and Canale's chemostat model, a bifurcation diagram comparing the maximum algal growth rate, b_C, and the inflow medium nitrogen concentration, N_i, is needed. It is easy to reliably generate this diagram using the IN/GB method and the techniques described in this paper. The bifurcation diagram is given in Fig. 9.

This diagram can be compared to Fig. 1 for the Rosenzweig-MacArthur model and Fig. 6 for Canale's chemostat model. The bifurcation curves are easily identifiable because along the lines $\delta = 0.08$ day^{-1} and $b_C = 3.3$ day^{-1}, Fig. 8 and Fig. 9 intersect. Thus, the order of the bifurcation curves is, from left to right, and bottom to top, TE, TE, H. The region of steady, stable coexistence is shown by the shaded area in Fig. 9. Initially this region seems dissimilar to the regions observed in Fig. 1 and Fig. 4. Recall that in the Rosenzweig-MacArthur model and in Canale's chemostat model, as the prey growth rate increased, the amount of enrichment needed to destabilize the coexisting state decreased. The opposite effect is predicted by the algae-rotifer model. This phenomena is, again, explained by the fact that the algae-rotifer model consists of only two trophic levels, while the other two models both feature three trophic levels. The rightmost transcritical and Hopf bifurcation curves in Fig. 9 can be thought of as being equivalent to the middle transcritical bifurcation and the planar Hopf bifurcation in Fig. 6. Thus the behavior of the coexisting state (nitrogen-algae-rotifer) of the algae-rotifer model matches the behavior observed in the nutrient-prey-predator subspace of Canale's model. The behavior of these spaces differs from the Rosenzweig-MacArthur model in that the limits of steady, stable coexistence for the prey-predator subspace in the Rosenzweig-MacArthur model do not depend on the prey growth rate, r, which can observed by the vertical planar Hopf bifurcation line and the vertical (leftmost) transcritical bifurcation in Fig. 1.

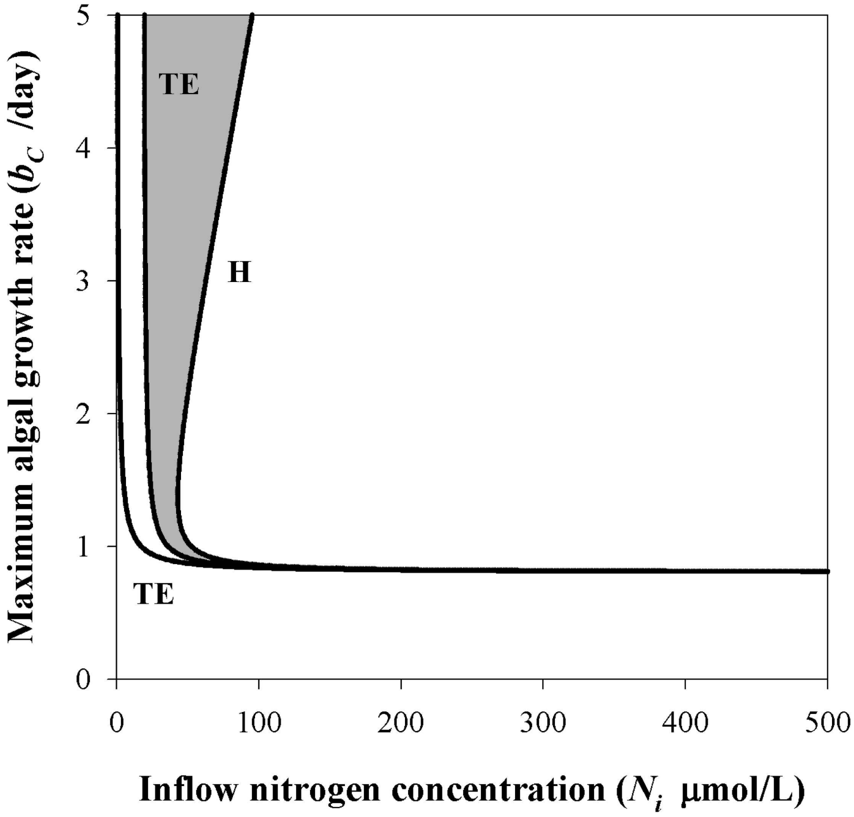

Fig. 9. Bifurcation of equilibrium diagram of inflow nitrogen concentration (N_i) versus maximum algal growth rate (b_C) for the algae-rotifer model with $\delta = 0.8/day$. TE: Transcritical of equilibrium; H: Hopf. Region of stable coexistence shaded in grey.

In order to compare the behavior predicted by the experimentally-verified algae-rotifer model with the behaviors predicted by the Rosenzweig-MacArthur model in Fig. 3 and by Canale's model in Fig. 7, a diagram comparing the maximum algal growth rate, b_C, with the rotifer mortality rate, m, is necessary. This diagram was generated using the IN/GB method, as before, and is given in Fig. 10.

In Fig. 10 there are three bifurcation curves present. There is a horizontal transcritical line at $b_C \approx 0.8344$, which matches the value of b_C at which the transcritical bifurcation occurs in Fig. 9 at $N_i = 100.0$. At values of b_C below this line, the only feasible state is a nutrient-only state. Crossing this transcritical bifurcation results in a nitrogen-algae state becoming both feasible and stable. This horizontal line in Fig. 10 indicates that there is a minimum value of the maximum algal growth rate b_C that is necessary to support a feasible algal population, and this value is not dependent on the rotifer mortality rate, which matches the behavior observed in Canale's model in Fig. 7.

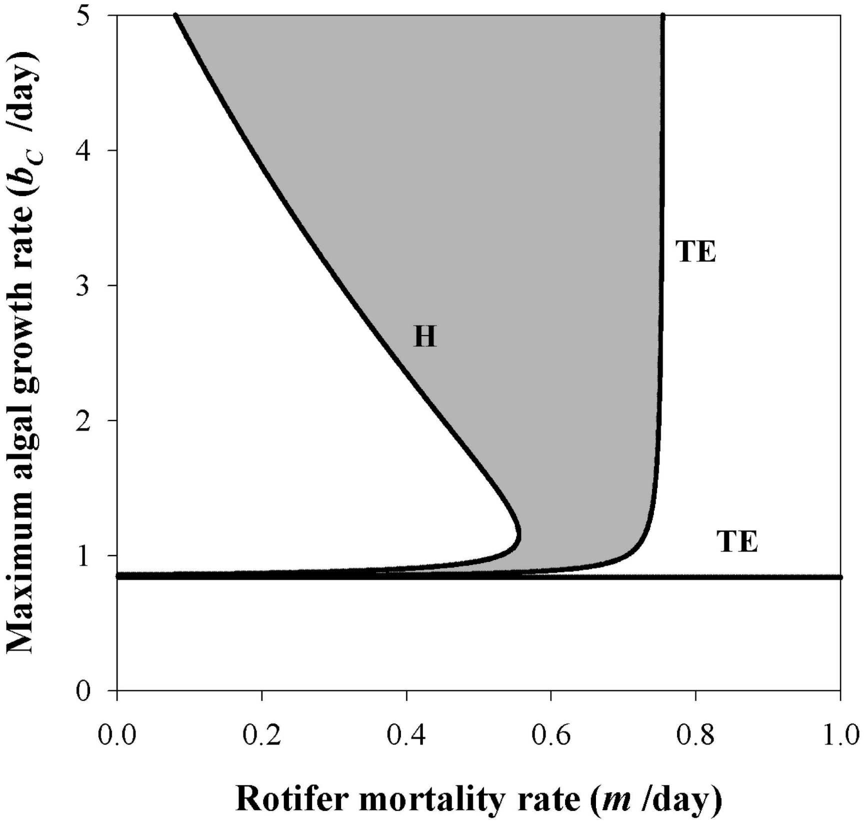

Fig. 10. Bifurcation of equilibrium diagram of rotifer mortality rate (m) versus maximum algal growth rate (b_C) for the algae-rotifer model with $\delta = 0.8/day$ and $N_i = 100.0\mu$mol/liter. TE: Transcritical of equilibrium; H: Hopf. Region of stable coexistence shaded in grey.

This behavior makes intuitive sense in that the behavior of the nutrient-prey (nitrogen-algae) subsystem should not depend on any model parameters that do not appear in that subsystem, which includes the predator (rotifer) mortality rate. The second transcritical bifurcation in Fig. 10 always occurs at values of b_C greater than the horizontal transcritical bifurcation. Crossing this bifurcation by either increasing b_C or by decreasing the rotifer mortality rate, m, results in a feasible and stable coexisting (nitrogen-algae-rotifer) steady state for this system. The last bifurcation in this diagram is a Hopf bifurcation. Crossing this bifurcation left to right by increasing the rotifer mortality rate, m, results in an unstable coexisting state becoming stable.

The region of coexisting stability is shown by the shaded area in Fig. 10. Recall that the algae-rotifer model only has two trophic levels while both Canale's model and the Rosenzweig-MacArthur model feature three levels. Therefore Hopf bifurcations in the algae-rotifer model should match planar Hopf bifurcations in the previous two models examined. Furthermore, the behavior of the coexisting state in the algae-rotifer model should match the behavior of the prey-predator subspace in the other two models. When Fig. 10 is compared to Fig. 7 we can immediately see that the behavior of the Hopf bifurcation in Fig. 10 matches the behavior of the planar Hopf bifurcation in Fig. 7. Crossing the planar Hopf bifurcation in Fig. 7 results in a change in stability of the nutrient-prey-predator subsystem; however, this stability change is not always observed due to the sign of the fourth eigenvalue. Furthermore, the second (non-horizontal) transcritical bifurcation in Fig. 10 matches the behavior of the rightmost transcritical bifurcation in Fig. 7. Therefore, the trends observed for the nutrient-prey-predator system are equivalent in the two models. In the Rosenzweig-MacArthur model, once again we see that the prey-predator subspace is bounded by a vertical planar Hopf bifurcation line and a vertical (rightmost) transcritical bifurcation in Fig. 3, and therefore this region, as observed previously, does not depend on the prey growth rate, r. This, of course, differs from the behavior observed for both Canale's model and the algae-rotifer model. However, it is easy to see that the two chemostat-based models behave quite similarly when the comparison is made between identical state spaces.

5 Concluding Remarks

Using several examples drawn from three different food chain models, we have demonstrated here the use of an interval-Newton method for the analysis of the nonlinear dynamical systems that arise in food chain modeling, specifically for computing all equilibrium states and bifurcations of equilibria (fold, transcritical, Hopf, double-fold and fold-Hopf). Using this method it was possible to easily, without any need for initialization or *a priori* insight into expected system behavior, generate complete solution branch diagrams and bifurcation of equilibria diagrams. This was done automatically, without requiring user interaction, a common need (Kuznetsov, 1998) in using continuation tools. Furthermore, this could be done with certainty, since the technique provides a mathematical and computational guarantee that all solutions to a system of nonlinear equations are enclosed. Since this technique is essentially initialization independent, beyond the setting of an initial interval for study, it can provide a powerful alternative to traditional continuation methods, which in general are initialization dependant and thus may not be completely reliable.

In principle, the interval method can be applied to compute the equilibrium states and bifurcations of equilibria in any continuous-time model of population dynamics in a food chain or food web, though in practice it is subject to some limitations, as discussed below. The advantages provided by the interval approach should make it particularly useful whenever analysis of a new model is undertaken, since this is the case in which initialization issues are most likely to arise in using traditional methods. For similar reasons, we have found the method to be very useful, as shown in the examples above, in working with existing models in parameter subspaces not analyzed previously.

We are particularly interested in the application of this method in the development and improvement of relatively small-scale food webs. There has been significant recent interest in modeling such systems and in studying their dynamics using bifurcation analysis. For example, Kooi and Kooijman (2000) developed a simple food network model that illustrates the effects of introducing a competitive species in the lowest trophic level. One- and two-parameter bifurcation diagrams in a parameter space describing the addition of nutrients to the system were used to show that introducing a competitive species to the prey trophic level can stabilize an oscillatory nutrient-prey-predator system. Kuijper et al. (2003) used a small-scale food web model to to investigate the effects of omnivory, or intraguild predation, in a chemostat. Bifurcation diagrams were computed to analyze the relationship between the extent of intraguild predation and the concentration of nutrient in the inflow, showing that omnivory can stabilize food chains, eliminate chaos, and give rise to multiple steady states. Kavadia et al. (2007) studied the dynamics of free-living, nitrogen-fixing bacterial populations under varying environmental and competitive conditions using a simple food network model. Bifurcation diagrams were used to illustrate the effects of altering system dilution rates and energy sources, with the conclusion that nitrogen-fixing populations can coexist with competitors under certain conditions of enrichment, but can be inhibited or destroyed when specific nutrient resources are low. In these examples, and in similar small-scale food network models, the interval approach can be applied to validate existing bifurcation diagrams and to compute new bifurcation diagrams for other parameter values or in other parameter subspaces. By providing a reliable and very easily used approach for determining one- or two-parameter bifurcation diagrams, the interval method also makes it easy to look at the effects of changing trophic interactions and response functions, as well as parameter values, and to thus study possible improvements in the models.

Despite the advantages of the interval technique described here, there are some practical limitations. An important limitation is that our current implementation of the interval-Newton method is not suitable for directly locating limit cycles and their bifurcations, which are very important dynamic features. By providing a reliable method for computing Hopf bifurcations, the interval method does provide a reliable means to initialize continuation methods for locating cycles (since a Hopf bifurcation corresponds to the appearance or disappearance of a limit cycle), and this is useful. This combination of interval and continuation methods should provide a reliable, though not guaranteed approach for locating limit cycles and their bifurcations. A fully interval method for limit cycles is being investigated, based in part on ideas provided by Galias

(2001, 2002).

Another limitation of the interval approach is in the problem size (number of state variables) that it can be applied to. This limitation is directly related to computation time requirements, and thus some discussion of the computational effort required to solve the example problems is needed. Average CPU times for the computation of fold and transcritical bifurcations ranged from 0.6 to 16 seconds per parameter iteration, while for computing Hopf bifurcations this figure was 1.4 to 100 seconds. Computing codimension-2 double fold and fold-Hopf bifurcation points required between 39 and 4800 seconds. The wide range of computation times is due to a variety of factors, including differences in the level of complexity between the models, as well as differences between computers used (all computations were done on either a 1.7 GHz or 3.4 GHz Intel CPU, under the Linux operating system using Intel Fortran Compiler 7.1). For the examples studied here we consider this level of computational effort to be quite reasonable, especially since the method used provides a guarantee of reliability, which other methods do not. Furthermore, since the diagrams can be generated automatically, without user intervention to deal with initialization issues, the elapsed time to generate a bifurcation diagram for a new model may actually be significantly less than when initialization-dependent methods are used. However, as problem size grows much beyond that considered here, the determination of two-parameter bifurcation diagrams using the interval method will become significantly more expensive computationally. This is due primarily due to the complexity involved in computing the determinant and bialternate product functions, and their derivatives, in Eqs. (15), (17), (20) and (21). On the other hand, the computation of equilibrium states was extremely fast for the models considered in this work, requiring less than 0.1 seconds of CPU time per parameter iteration. This suggests that it should be possible to compute solution branch diagrams for much larger systems. We have recently demonstrated this by using the interval method to compute all the equilibrium states in a nonlinear 17-variable food web model Gwaltney et al. (2006).

6 Acknowledgments

This work was supported in part by the Department of Education Graduate Assistance in Areas of National Needs (GAANN) Program under Grant #P200A010448, by the State of Indiana 21st Century Research and Technology Fund under Grant #909010455 and by the National Oceanic and Atmospheric Administration under Grant #NA050AR4601153.

References

Abrams, P.A., Roth, J.D., 1994. The effects of enrichment of three-species food chains with non-linear functional responses. Ecology, 75, 1118–1130.

Bartell, S.M., Gardner, R., and O'Neill, R., 1992. Ecological Risk Estimation. Lewis Publishers, Ann Arbor, MI, 272 pp.

Bernot, R.J., Kennedy, E.E., Lamberti, G.A., 2005. Effects of ionic liquids on the survival, movement, and feeding behavior of the freshwater snail, *Physa acuta*. Environ. Toxicol. Chem., 24, 1759–1765.

Bernot, R.J., Brueseke, M.A., Evans-White, M.A., Lamberti, G.A., 2005. Acute and chronic toxicity of imidazolium-based ionic liquids on *Daphnia magna*. Environ. Toxicol. Chem., 24, 87–92.

Bischof, C.H., Lang, B., Marquardt, W., Mönnigmann, M., 2000. Verified determination of singularities in chemical processes. Proc. SCAN 2000, 9th GAMM-IMACS International Symposium on Scientific Computing, Computer Arithmetic, and Validated Numerics, Sept. 18-22, 2000, Karlsruhe, Germany.

Boer, M.P., Kooi, B.W., Kooijman, S.A.L.M, 1998. Food chain dynamics in the chemostat. Math. Biosci., 150, 43–62.

Brennecke, J.F., Maginn, E.J., 2001. Ionic liquids: Innovative fluids for chemical processing. AIChE J., 47, 2384–2389.

De Feo, O., Rinaldi, S., 1997. Yield and dynamics of tritrophic food chains. Am. Nat., 150, 328–345.

Dhooge, A., Govaerts, W., Kuznetsov, Y.A., 2003. MATCONT: A MATLAB package for numerical bifurcation analysis of ODEs. ACM Trans. Math. Softw., 29, 141–164.

Docherty, K.M, Kulpa, C.F., 2005. Toxicity and antimicrobial activity of imidazolium and pyridinium ionic liquids. Green Chem., 7, 185–189.

Doedel, E.J., Paffenroth, R.C., Champneys, A.R., Fairgrieve, T.F., Kuznetsov, Y.A., Oldeman, B.E., Sandstede, B., 2002. AUTO 2000: Continuation and bifurcation software for ordinary differential equations (with HomCont). User's Guide. Available with software at http://sourceforge.net/projects/auto2000.

El-Sheikh, M.M.A., Mahrouf, S.A.A., 2005. Stability and bifurcation of a simple food chain in a chemostat with removal rates. Chaos Solitons Fractals, 23, 1475–1489.

Fussmann, G.F., Ellner, S.P., Shertzer, K.W., Hairston, N.G., 2000. Crossing the Hopf bifurcation in a live predator-prey system. Science, 290, 1358–1360.

Galias, Z., 2001. Interval methods for rigorous investigation of periodic orbits. International Journal of Bifurcation and Chaos, 11, 2427–2450.

Galias, Z., 2002. Proving the existence of long periodic orbits in 1D maps using Interval-Newton method and backward shooting. Topology and its Applications, 124, 25–37.

Gau, C.-Y., Stadtherr, M.A., 2002. New interval methodologies for reliable chemical process modeling. Comput. Chem. Eng., 26, 827–840.

Gehrke, V., Marquardt, W., 1997. A singularity theory approach to the study of reactive distillation. Comput. Chem. Eng., 21(Suppl.), S1001–S1006.

Gorman-Lewis, D.J., Fein, J.B., 2004. Experimental study of the adsorption of an ionic liquid onto bacterial and mineral surfaces. Environ. Sci. Technol., 38, 2491–2495.

Govaerts, W.J.F., 2000. Numerical Methods for Bifurcations of Dynamical Equilibria. SIAM, Philadelphia, 362 pp.

Gragnani, A., De Feo, O., Rinaldi, S., 1998. Food chains in the chemostat: Relationships between mean yield and complex dynamics. Bull. Math. Biol., 60, 703–719.

Gwaltney, C.R., Styczynski, M.P., Stadtherr, M.A., 2004. Reliable computation of equilibrium states and bifurcations in food chain models. Comput. Chem. Eng., 28, 1981–1996.

Gwaltney, C.R., Stadtherr, M.A., 2006. Reliable computation of equilibrium states and bifurcations in nonlinear dynamics. Lecture Notes in Computer Science, 3732, 122–131.

Gwaltney, C.R., Schmitz, R.A, Stadtherr, M.A., 2006. Computation of equilibrium states in food network models using interval analysis. Presented at AIChE Annual Meeting, San Francisco, CA, November 12-17, 2006.

Hansen, E.R., Walster, G.W., 2004. Global Optimization Using Interval Analysis. Marcel Dekker, New York, 728 pp.

Hastings, A., Powell, T., 1991. Chaos in a three-species food chain. Ecology, 72, 896–903.

Kavadia, A., Vayenas, D.V., Pavlou, S., Aggelis, G., 2007. Dynamics of free-living nitrogen-fixing bacterial populations in antagonistic conditions. Ecological Modelling, 200, 243–253.

Kearfott, R.B., 1996. Rigorous Global Search: Continuous Problems. Kluwer, Dordrecht, The Netherlands, 261 pp.

Klebanoff, A., Hastings, A. 1994. Chaos in three-species food chains. J. Math. Biol., 32, 427–451.

Kooi, B.W., Boer, M.P., Kooijman, S.A.L.M., 1997a. Complex dynamic behavior of autonomous microbial food chains. J. Math. Biol., 36, 24–40.

Kooi, B.W., Boer, M.P., Kooijman, S.A.L.M., 1997b. Mass balance equation versus logistic equation in food chains. J. Biol. Sys., 5, 77–85.

Kooi, B.W., Boer, M.P., Kooijman, S.A.L.M., 1998. On the use of the logistic equation in models of food chains. Bull. Math. Biol., 60, 231–246.

Kooi, B.W., Kooijman, S.A.L.M., 2000. Invading species can stabilize simple trophic systems. Ecological Modelling, 133, 57–72.

Kooi, B.W., 2003. Numerical bifurcation analysis of ecosystems in a spatially homogeneous environment. Acta Biotheor., 51, 189–222.

Kuijper, L.D.J., Kooi, B.W., Zonneveld, C., Kooijman, S.A.L.M., 2003. Omnivory and food web dynamics. Ecological Modelling, 163, 19–32.

Kuznetsov, Y.A., Rinaldi, S. 1996. Remarks on food chain dynamics. Math. Biosci., 134, 1–33.

Kuznetsov, Y.A., 1998. Elements of Applied Bifurcation Theory. Springer-

Verlag, New York, 515 pp.

Jaulin, L., Kieffer, M., Didrit, O., Walter, É., 2001. Applied Interval Analysis. Springer-Verlag, London, 384 pp.

Makino, K., Berz, M., 2003. Taylor models and other validated functional inclusion methods. Int. J. Pure Appl. Math., 4, 379–456.

Moghadas, S.M., Gumel, A.B., 2003. Dynamical and numerical analysis of a generalized food-chain model. Appl. Math. Comput., 142, 35–49.

Mönnigmann, M., Marquardt, W., 2002. Normal vectors on manifolds of critical points for parametric robustness of equilibrium solutions of ODE systems. J. Nonlinear Sci., 12, 85–112.

Moore, R.E., 1966. Interval Analysis. Prentice-Hall, Englewood Cliffs, NJ, 145 pp.

Naito, W., Miyamoto, K., Nakanishi, J., Masunaga, S., Bartell, S., 2002. Application of an ecosystem model for aquatic ecological risk assessment of chemicals for a Japanese lake. Water Res., 36, 1–14.

Neumaier, A., 1990. Interval Methods for Systems of Equations. Cambridge Univ. Press, Cambridge, U.K., 255 pp.

Pernak, J., Sobaszkiewicz, K., Mirska, I., 2003. Anti-microbial activities of ionic liquids. Green Chem., 5, 52–56.

Ranke, J., Molter, K., Stock, F., Bottin-Weber, U., Poczobutt, J., Hoffmann, J., Ondruschka, B., Filser, J., Jastorff, B., 2004. Biological effects of imidazolium ionic liquids with varying chain lengths in acute *Vibrio fischeri* and WST-1 cell viability assays. Ecotox. Environ. Safe., 58, 396–404.

Ropel, L., Belvèze, L.S., Aki, S.N.V.K., Stadtherr, M.A., Brennecke, J., 2005. Octanol-water partition coefficients of imidazolium-based ionic liquids. Green Chem., 7, 83–90.

Schnepper, C.A., Stadtherr, M.A., 1996. Robust process simulation using interval methods. Comput. Chem. Eng., 20, 187–199.

Seydel, R., 1988. From Equilibrium to Chaos: Practical Bifurcation and Stability Analysis. Elsevier, New York, NY, 367 pp.

Stepnowski, P., Skladanowski, A.C., Ludwiczak, A., Laczynska, E., 2004. Evaluating the cytotoxicity of ionic liquids using human cell line HeLa. Hum. Exp. Toxicol., 23, 513–517.

Turchin, P., 2003. Complex Population Dynamics: A Theoretical/Empirical Synthesis. Princeton Univ. Press, Princeton, NJ, 450 pp.